Nuclear Moments in Density Functional Theory

An analysis of magnetic dipole and electric quadrupole moments within nuclear DFT of one-particle and one-hole neighbours of doubly magic nuclei

Paolo Livio Sassarini

Master of Philosophy

University of York
Physics, Engineering and Technology
September 2023

Abstract

The density functional theory (DFT) code, HFODD, was used to calculate magnetic dipole μ and electric quadrupole Q moments, with emphasis on the former, of the odd neighbours of eight doubly magic nuclei (^{16}O, ^{40}Ca, ^{48}Ca, ^{56}Ni, ^{78}Ni, ^{100}Sn, ^{132}Sn and ^{208}Pb).

In our approach, we made use of pure Hartree-Fock using the Skyrme and Gogny functionals while aligning the angular momenta along the axial-symmetry axis and breaking time-reversal symmetry, which allowed for a full analysis of the spin polarization effects due to the unpaired nucleon. In order to restore the broken symmetries, the projection-after-variation (PAV) method was used which provides us with the spectroscopic moments. Our results were achieved by adjusting one coupling constant in the time-odd mean-field sector of the nuclear functional, namely the time-odd spin-spin isovector Landau parameter g_0'. The results were compared with experimental data, where available, to determine the validity of our work.

From the analysis, we have concluded that our approach is promising and stands as a solid base for further work into the area and allowing the opportunity to refine the work through additional approaches e.g. deformed-configuration interaction. We note that as a consequence of our work, we determined that the use of effective charges and effective g-factors are not needed to describe the nuclear moments.

Contents

List of Figures

List of Tables

List of abbreviations

DFT	Density Functional Theory
HF	Hartree-Fock
BCS	Bardeen-Cooper-Schrieffer
HFB	Hartree-Fock-Bogoliubov
AMP	Angular Momentum Projection
VAP	Variation-after-projection
PAV	Projection-after-variation
MEC	Meson Exchange Currents
BMF	Beyond Mean-Field
HO	Harmonic Oscillator
s.p.	Single-Particle
SCCM	Symmetry Conserving Configuration Mixing
CDFT	Covariant Density Functional Theory
RPA	Random Phase Approximation
EXP	Experiment

Acknowledgements

- I would first like to thank my supervisor, Professor Jacek Dobaczewski, for providing me with the opportunity to work with him. His supervision was flawless from start to finish and I will be forever grateful for his time.
- A massive thank you to my parents, Margaret and Archie, for their full and constant support throughout my studies. Without their help, I would not have got this far.
- A special thanks to my brother and sister; Massimo and Daria, and their partners; Caitlin and Alasdair.
- I also need to thank the friends I made at York. I will always remember the "discussions" in the office, the pub sesh's and all laughs we had together.
- Finally, many thanks to Antonio for his help with the formatting.

Author's Declaration

I declare that this thesis is a presentation of original work and I am the sole author. This work has not previously been presented for an award at this, or any other, University. All sources are acknowledged as References.

The present work lead to the publication of the following original article:

- P. L. Sassarini, J. Dobaczewski, J. Bonnard and R. F. Garcia Ruiz. "Nuclear DFT analysis of electromagnetic moments in odd near doubly magic nuclei". Journal of Physics G: Nuclear and Particle Physics 49 (2022) 11LT01.

Chapter 1

Introduction

1.1 History

Ernest Rutherford's discovery of the atomic nucleus in his famous α-particle scattering experiment in 1911 led to the birth of nuclear physics [Rut11]. This in turn allowed for the proposal of one of the earliest models of nuclear structure, the so-called liquid drop model, which then led to the formulation of the semi-empirical mass formula by Carl Friedrich von Weizsäcker [Wei35]. This formula allows for a simple calculation producing a fairly good approximation for the binding energy of the nucleus, which we know to be a complex quantum many-body system.

These advancements led to the study of nuclear moments, starting with the measurements of magnetic moments in the 1950's with the development of nuclear magnetic resonance (NMR) spectroscopy and then later the measurements of electric moments in the 1970's from the hyperfine structure of muonic x-rays [Ney03].

This has aided in our understanding of the structure of the atomic nucleus and has led to the development of many theoretical models describing the properties of the nucleus, including those discussed in this thesis.

1.2 Past Research

There have been multiple contributions to the study of nuclear structure with regards to nuclear moments using nuclear density functional theory (DFT) and had great success. However, these studies have had limitations with which regions of the nuclear landscape that can be modelled and most often require adjustments to describe different regions. The following list shows the groups, to date, that have done major work in the field relating to this subject.

- M. Borrajo and J. L. Egido [BE16] [BE17] [BE18a] [BE18b].
- S. Péru, S. Hilaire, S. Goriely and M. Martini [Pér21].
- L. Bonneau, P. Quentin, N. Minkov and J. Bartel [Bon12] [Bon15].
- J. Li, J. Meng and J. Wei [WLM12] [LM18].
- G. Co', V. De Donno, M. Anguiano, R. N. Bernard and A. M. Lallena [Co15].

More details on each group's approach will be discussed in Chapter 8.

Chapter 2

Nuclear Structure

2.1 Nuclear Shell Model

2.1.1 Magic Numbers

To begin with, the inspiration for the nuclear shell model came from the atomic shell model for the electrons in the atom. One of the main indicators for a shell structure in the nucleus is the very apparent maxima of neutron separation energies of specific numbers of nucleons [VHZ01]. This indicated closed shells at specific numbers; 2, 8, 20, 28, 50, 82 and 126.

Further evidence to suggest a shell model and these magic numbers is the experimental data on the excitation energy of the first excited states of even-even nuclei [Hey04], further confirming these magic numbers (126 for neutrons only) and a shell structure.

2.1.2 Spherical Shell Model

The spherical shell model is produced by solving the three-dimensional Schrödinger equation:

$$\left[-\frac{\hbar^2}{2m}\Delta_i + U(r)\right]\phi_i(\vec{r}) = E\phi_i(\vec{r}) \ , \tag{2.1}$$

where $U(r)$ is a radial-symmetric potential, $\phi_i(\vec{r})$ is the single-particle wavefunction of the i-th particle, E is the energy and Δ is the Laplace operator, defined as, $\Delta = \vec{\nabla}^2 = \frac{\partial^2}{\partial x^2} + \frac{\partial^2}{\partial y^2} + \frac{\partial^2}{\partial z^2}$.

When choosing a potential, it is wise to look to experimental data to determine which will model the physics the best. A suitable and widely used potential is the Woods-Saxon potential U_{WS} [WS54]:

$$U_{WS} = \frac{-U_0}{1 + e^{\frac{r-R}{a}}} \ , \tag{2.2}$$

where U_0 is the depth of the potential, r is the distance from the nucleus, R is the nuclear radius and a represents the skin thickness. These are usually chosen as $R = 1.25A^{1/3}$fm, $a = 0.524$fm and $U_0 \approx 50$MeV.

This is regarded as a good approximation for the potential as it reflects the properties of the matter distribution measured in electron scattering experiments. The only problem with this potential is that it can only be solved numerically. Due to this, an easily solvable harmonic oscillator potential, $U_{HO} = \frac{m\omega^2 r^2}{2}$, is usually used and conserves most of the physics. This is seen by the harmonic oscillator predicting the low magic numbers [Kra88].

After solving the three-dimensional Schrödinger equation using the harmonic oscillator potential, we get the energy eigenstates which are only dependent on the radial quantum number n and orbital angular momentum l:

$$E_{nl} = (2(n-1) + l)\hbar\omega + \frac{3}{2}\hbar\omega \ , \tag{2.3}$$

where $3/2\hbar\omega$ is present due to the uncertainty principle ($n \neq 0$).

This approach only produces the lower magic numbers and produces a degeneracy for different levels where $n = l$, however this can be improved on by introducing a residual interaction to the potential in the form of the spin-orbit interaction governed by $\vec{l} \cdot \vec{s}$. Through this method, we are able to split all levels dependent on their orbital angular momentum l and spin s.

As the spin-orbit interaction is mainly the scalar product of the orbital angular momentum and spin operators, the total angular momentum $\vec{j} = \vec{l} + \vec{s}$ is introduced to deal with this. Therefore, the expectation value is determined using the eigenvalues of each of the operators [Hey04]:

$$\langle \vec{l} \cdot \vec{s} \rangle = \frac{\hbar^2}{2} \left[j(j+1) - l(l+1) - s(s+1) \right] \ . \tag{2.4}$$

Our spin $s = \frac{1}{2}$ system results in couplings $j_+ = l + s = l + \frac{1}{2}$ and $j_- = l - s = l - \frac{1}{2}$.

Hence:

$$\begin{aligned} j_+ = l + s &= (l + \tfrac{1}{2}) \cdot (l + \tfrac{3}{2}) - l(l+1) - \tfrac{3}{4} \\ &= l \ , \end{aligned} \tag{2.5}$$

and,

$$\begin{aligned} j_- = l - s &= (l - \tfrac{1}{2}) \cdot (l + \tfrac{1}{2}) - l(l+1) - \tfrac{3}{4} \\ &= -(l+1) \ . \end{aligned} \tag{2.6}$$

Therefore:

$$\langle \vec{l} \cdot \vec{s} \rangle = \begin{cases} \frac{\hbar^2}{2} l, & \text{for} \quad j_+ \\ -\frac{\hbar^2}{2}(l+1), & \text{for} \quad j_- \ . \end{cases} \tag{2.7}$$

From Equation (2.7), it is easy to see that spin-orbit splitting increases as the orbital angular momentum l increases.

Therefore the energy eigenstates become:

$$E_{nl} = (2(n-1) + l)\hbar\omega + \frac{3}{2}\hbar\omega - \begin{cases} l & \text{for} \quad j_+ \\ -(l+1) & \text{for} \quad j_- \ . \end{cases} \tag{2.8}$$

It is now possible to construct an accurate shell model by using modifications from the realistic Woods-Saxon potential and adding the spin-orbit splitting, shown in Figure (2.1).

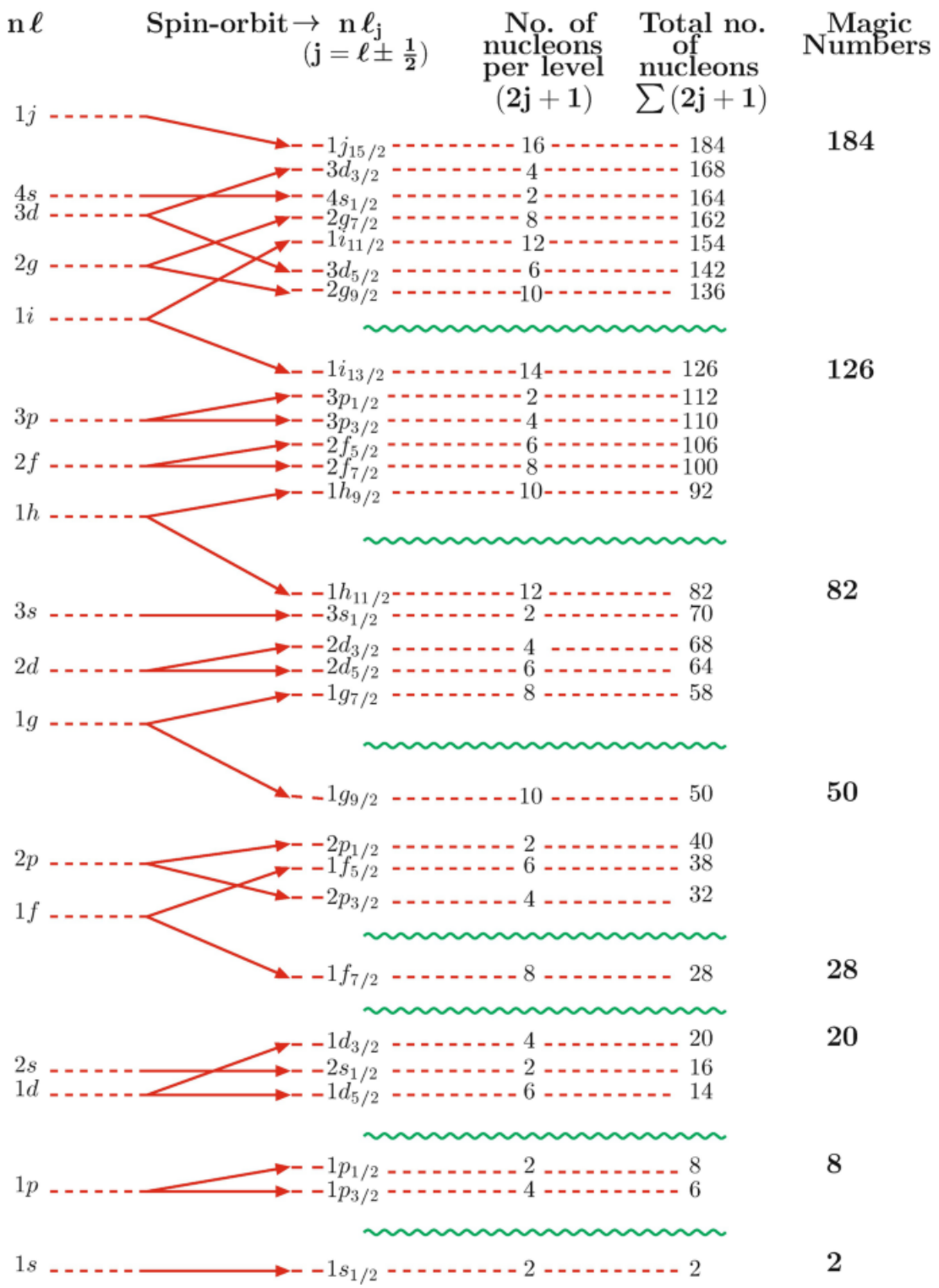

Figure 2.1: The nuclear shell model showing the full splitting of all levels from the spin-orbit interaction [BD21].

2.2 Nilsson Model

To account for deformations in nuclei, we shall introduce varying parameters on the spatial coordinates of a potential to best represent the deformation by an ellipsoidal distribution. This was first introduced by Sven Gösta Nilsson in 1955 [Nil55]. Using the harmonic oscillator, we see that the oscillators frequency of each axis can be differed and will produce this desired ellipsoidal distribution.

Therefore, using Cartesian coordinates, we have the potential as follows:

$$V(r) = \frac{m}{2}(\omega_x^2 x^2 + \omega_y^2 y^2 + \omega_z^2 z^2) \ . \tag{2.9}$$

The basic Hamiltonian can now be written as follows:

$$\hat{H} = -\frac{\hbar^2}{2m}\Delta + \frac{m}{2}(\omega_x^2 x^2 + \omega_y^2 y^2 + \omega_z^2 z^2) \ . \tag{2.10}$$

We must choose these frequencies ω carefully, these are determined to be proportional to the inverse of the half axes of the ellipsoid [Hey04]:

$$\omega_i = \mathring{\omega}_0 \frac{R_0}{a_i}, \quad (i \equiv x, y, z) \ , \tag{2.11}$$

with, $R_0 = 1.25$fm and a_i is the distance from the origin to the i-axis intercept.

We can state the eigenstates (n_x, n_y, n_z) and eigenvalues from the 1D-Harmonic Oscillator:

$$\epsilon_o(n_x, n_y, n_z) = \hbar\omega_x(n_x + \tfrac{1}{2}) + \hbar\omega_y(n_y + \tfrac{1}{2}) + \hbar\omega_z(n_z + \tfrac{1}{2}) \ . \tag{2.12}$$

Due to the incompressibility of nuclear matter, we are required to preserve the condition of volume conservation [GM96]. This is as follows:

$$\omega_x\omega_y\omega_z = \mathring{\omega}_0^3 = constant \ . \tag{2.13}$$

As our specific cases have axial symmetry around the z-axis, we can use cylindrical coordinates to simplify the derivation of the eigenvalues. We are now able to define small deviations on each axis by the use of a deformation parameter:

$$\omega_x^2 = \omega_y^2 = \omega_0^2(1 + \tfrac{2}{3}\delta) \ , \tag{2.14}$$

$$\omega_z^2 = \omega_0^2(1 - \tfrac{4}{3}\delta) \ , \tag{2.15}$$

with, $\omega_0 = \mathring{\omega}_0(1 - \frac{4}{3}\delta^2 - \frac{16}{27}\delta^3)^{-\frac{1}{6}}$.

Here we now define a new parameter, $b(\delta) = (\hbar/m\omega_0(\delta))^{\frac{1}{2}}$, which will give the coordinates of the system a representation in which they are dimensionless, expressed with a prime, $r' = r/b$. This is referred to as a deformation dependent oscillator length and the Hamiltonian is now able to be expressed, with a term relating to quadrupole deformation containing the relevant spherical harmonic $Y_{20}(\hat{r}')$ [Hey04]:

$$\hat{H}(\delta) = \hbar\omega_0(\delta)\left(-\frac{1}{2}\Delta' + \frac{r'^2}{2} - \frac{1}{3}\sqrt{\frac{16\pi}{5}}\delta r'^2 Y_{20}(\hat{r}')\right) \ . \tag{2.16}$$

From the liquid drop model, we can relate the deformation parameter, β, with this new parameter, δ. As we have ellipsoidal surfaces, we can say that the dimensionless coordinate, r', can be expressed as:

$$r' \sim (1 + \beta Y_{20}(\theta', \phi')) \ , \tag{2.17}$$

where,

$$\beta \approx \frac{1}{3}\sqrt{\frac{16\pi}{5}}\delta \approx 1.057\delta \ , \tag{2.18}$$

therefore, it can be said that $\beta \approx \delta$.

We have to now define the eigenstates using new quantum numbers:

$$N = n_x + n_y + n_z = n_z + 2n_\rho + m_l \ , \tag{2.19}$$

where m_l is the projection of the orbital angular momentum on the z-axis.

Therefore, by using Equation (2.12), we can now get the eigenvalues:

$$\begin{aligned} \epsilon_\delta(n_z, n_\rho, m_l) &= \hbar\omega_z(n_z + \tfrac{1}{2}) + \hbar\omega_\perp(2n_\rho + m_l + 1) \\ &\simeq \hbar\mathring{\omega}_0\left[(N + \tfrac{3}{2}) + \delta(\tfrac{N}{3} - n_z)\right] \ . \end{aligned} \tag{2.20}$$

From the axial symmetry, m_l becomes a good quantum number and therefore so is the spin component, s_z. Hence, the eigenvalue for the total angular momentum projection, $j_z \equiv \Omega$, can be defined:

$$\Omega = m_l + m_s = m_l \pm \frac{1}{2} \ . \tag{2.21}$$

Now we are able to characterise a deformed eigenstate of the Hamiltonian in the cylindrical

basis by this set of quantum numbers, also known as Nilsson quantum numbers [RS04]:

$$\Omega^{\pi}[Nn_z m_l] \ , \tag{2.22}$$

where π is the parity, calculated as $\pi = (-1)^l = (-1)^N$.

This model presented so far is very good at showing the major effects of nuclear deformation, however, it is unable to produce a realistic single-particle spectrum. In order to achieve this, more terms must be added to the Hamiltonian. We must add the spin-orbit to reproduce the magic numbers and add the $l^2 - \langle \hat{l}^2 \rangle_N$ term to 'flatten' the potential at higher l values, near the surface, as the harmonic oscillator potential fails to give the correct compression of these states.

We now define this new upgraded Hamiltonian [Hey04]:

$$\hat{H}_{Nilsson} = \hbar\omega_0(\delta)\left(-\frac{1}{2}\Delta' + \frac{r'^2}{2} - \beta r'^2 Y_{20}(\hat{r'})\right) - \kappa\hbar\mathring{\omega}_0\left(2\hat{l}\cdot\hat{s} + \mu(\hat{l}^2 - \langle\hat{l}^2\rangle_N)\right) \ , \tag{2.23}$$

where, κ is a parameter describing the spin-orbit strength and μ is an adjustable parameter used to shift the higher l states. For large deformations, the l^2 and $\langle \hat{l}^2 \rangle_N$ terms are neglected due to the over-powering effect that the quadrupole deformation has.

Presented below are all Nilsson plots used in the analysis to confirm the occupied states.

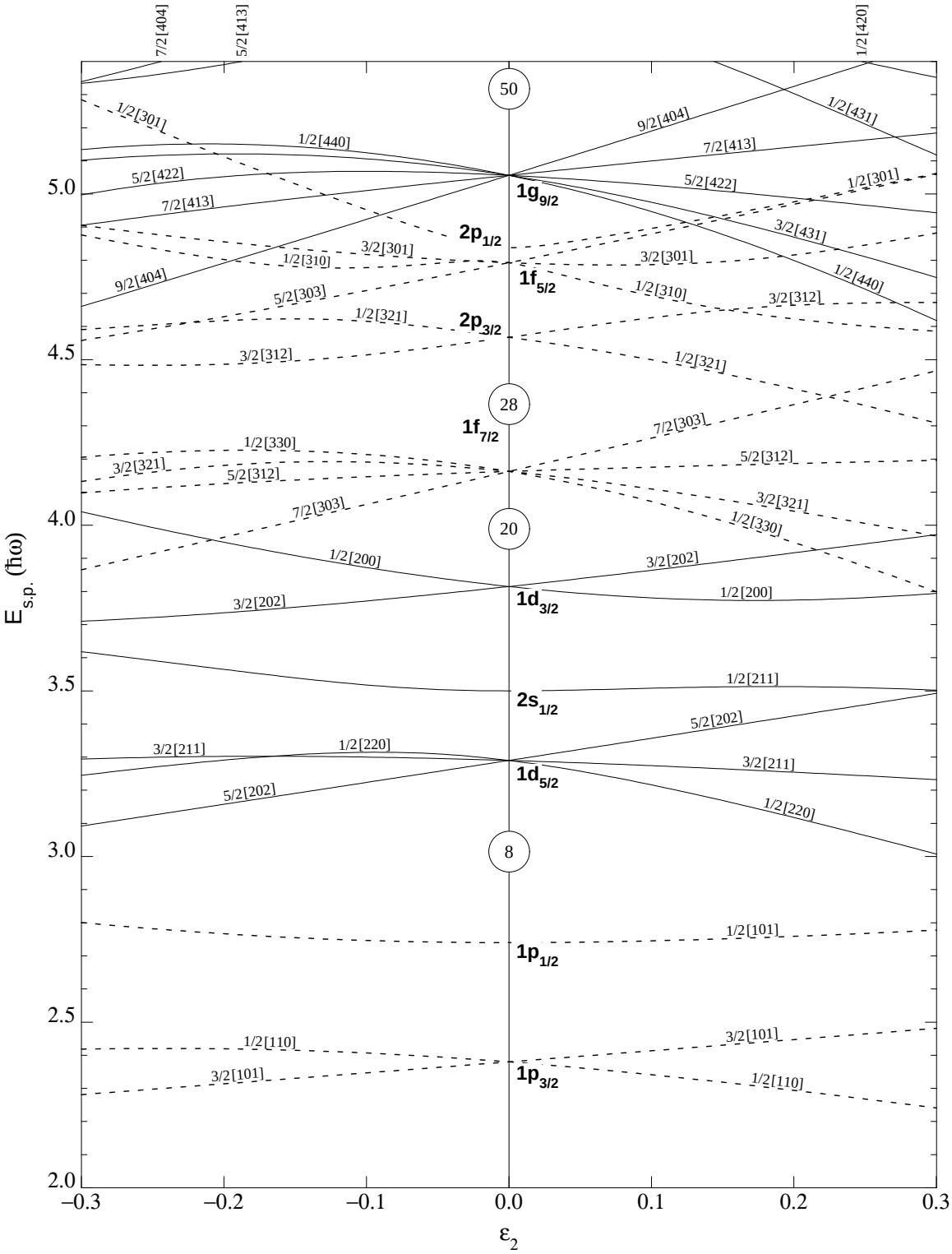

Figure 2.2: Nilsson diagram for protons or neutrons, Z or N $\leq$ 50 [Fir97].

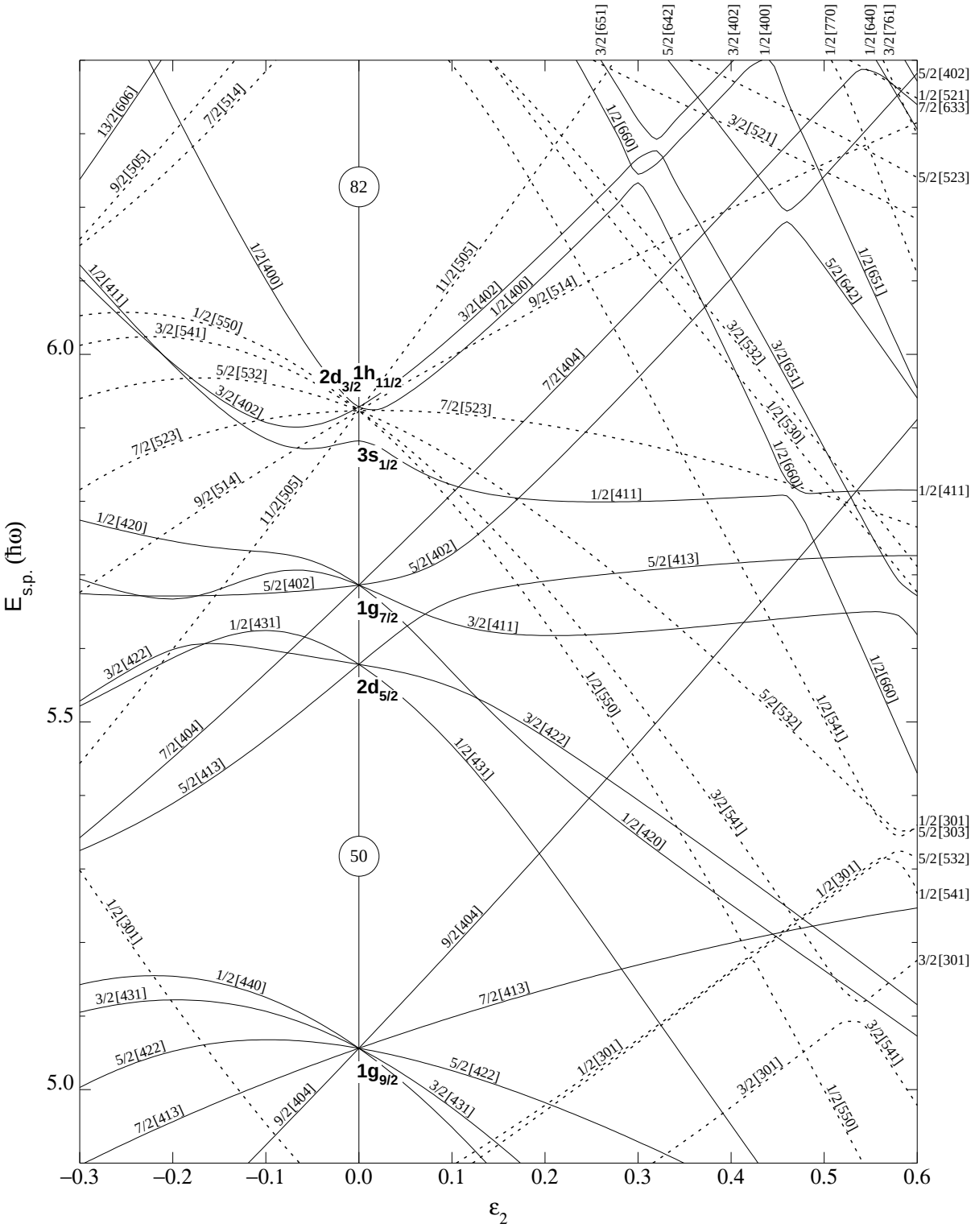

Figure 2.3: Nilsson diagram for neutrons, $50 \leq N \leq 82$ [Fir97].

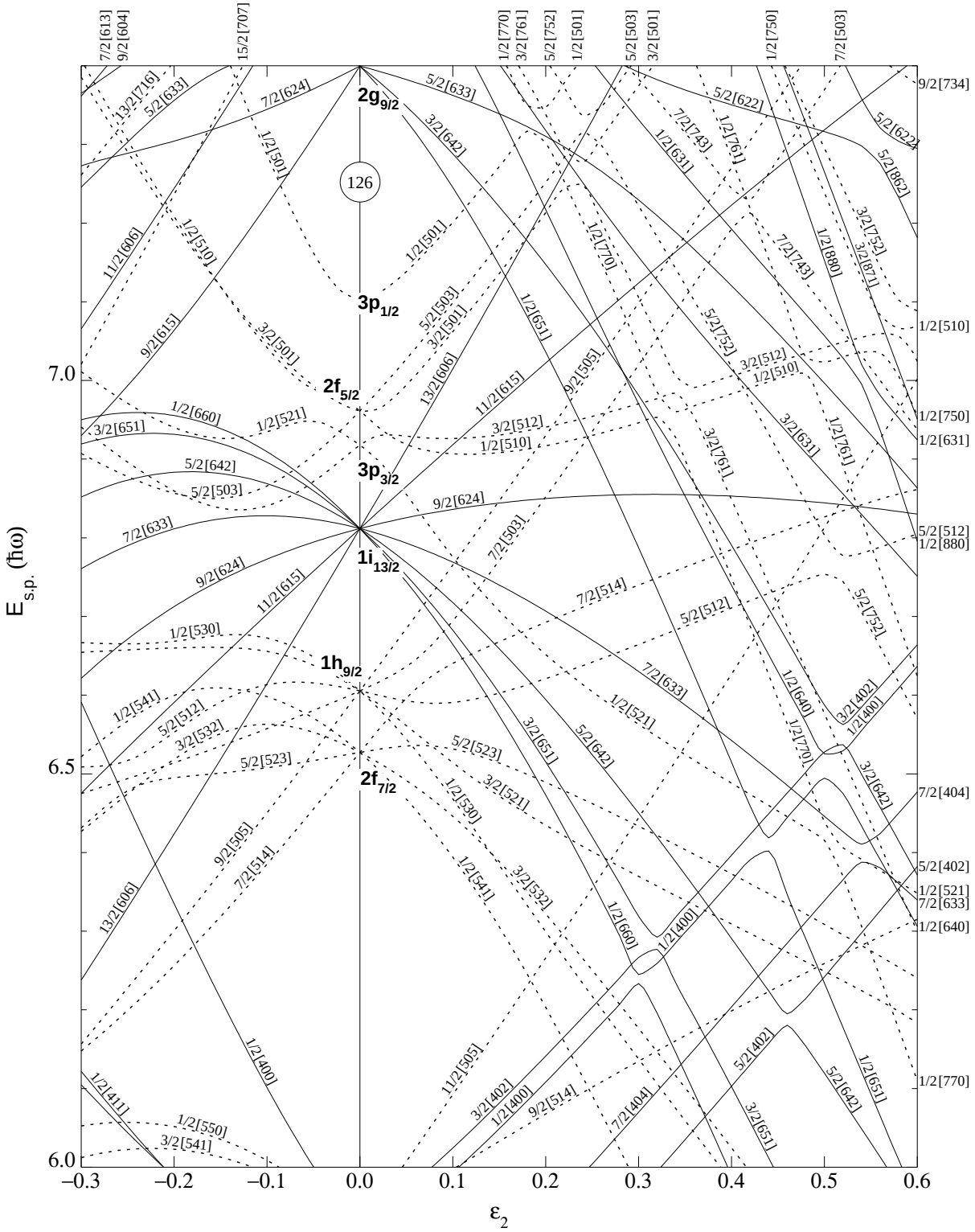

Figure 2.4: Nilsson diagram for neutrons, $82 \leq N \leq 126$ [Fir97].

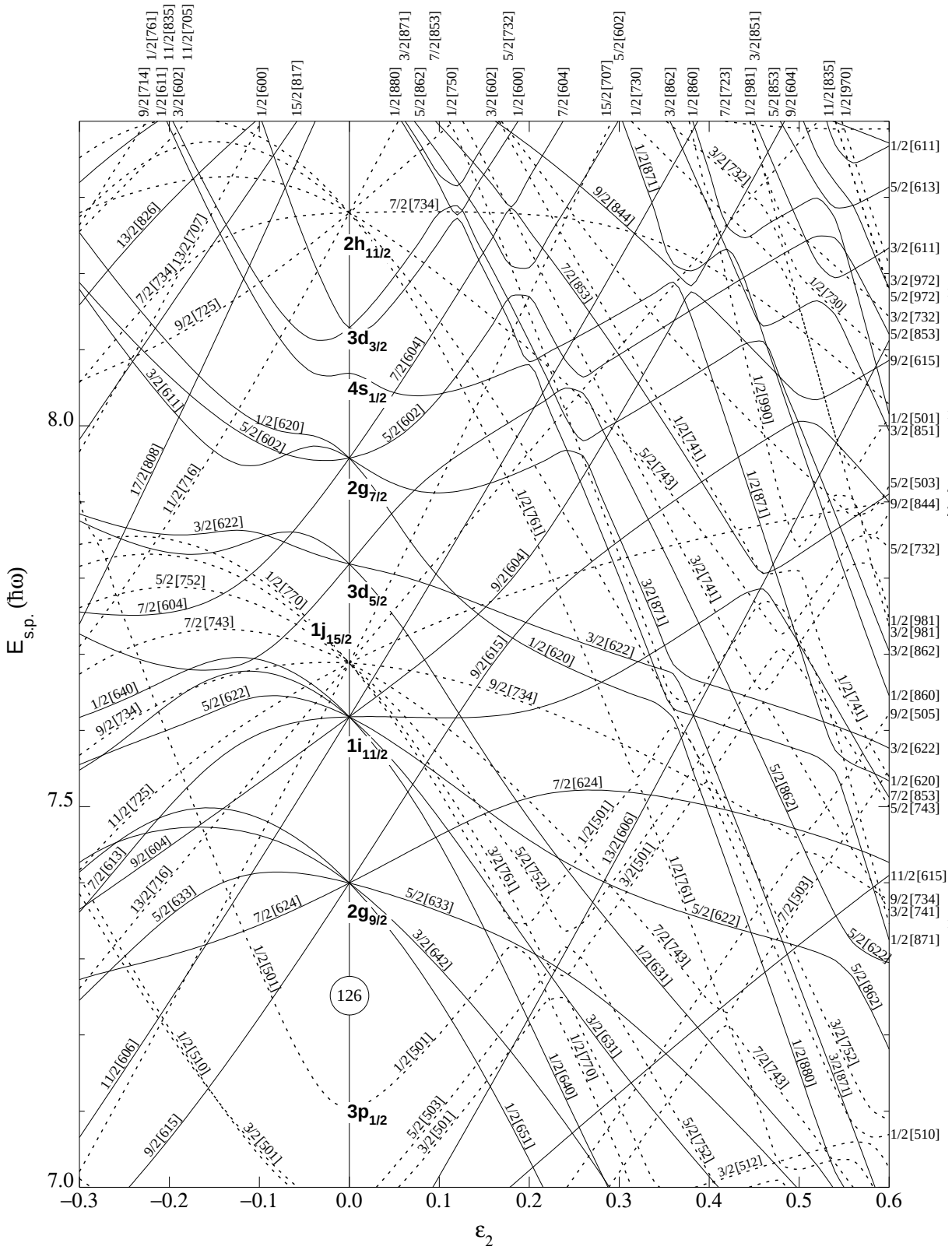

Figure 2.5: Nilsson diagram for neutrons, N $\geq$ 126 [Fir97].

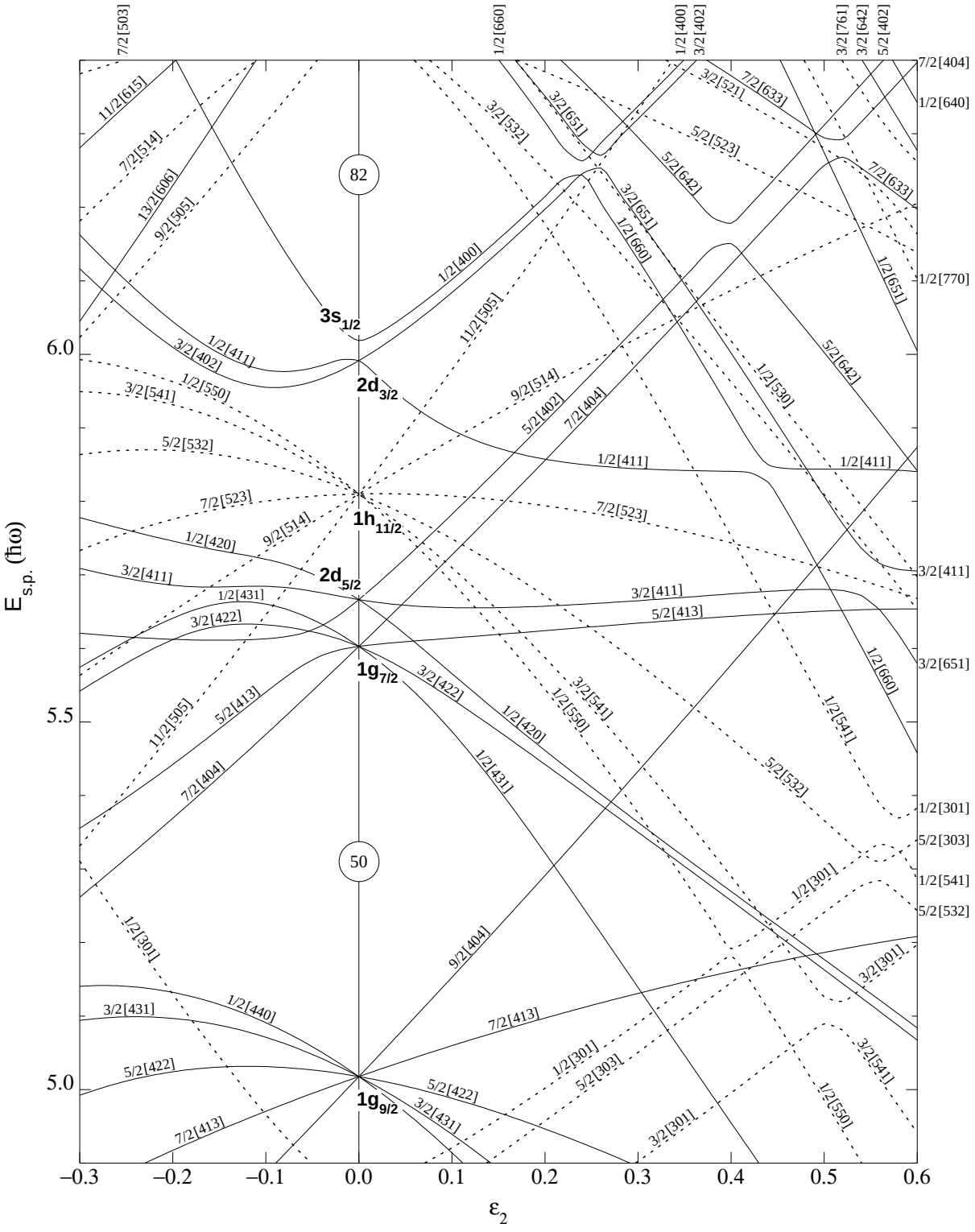

Figure 2.6: Nilsson diagram for protons, $50 \leq Z \leq 82$ [Fir97].

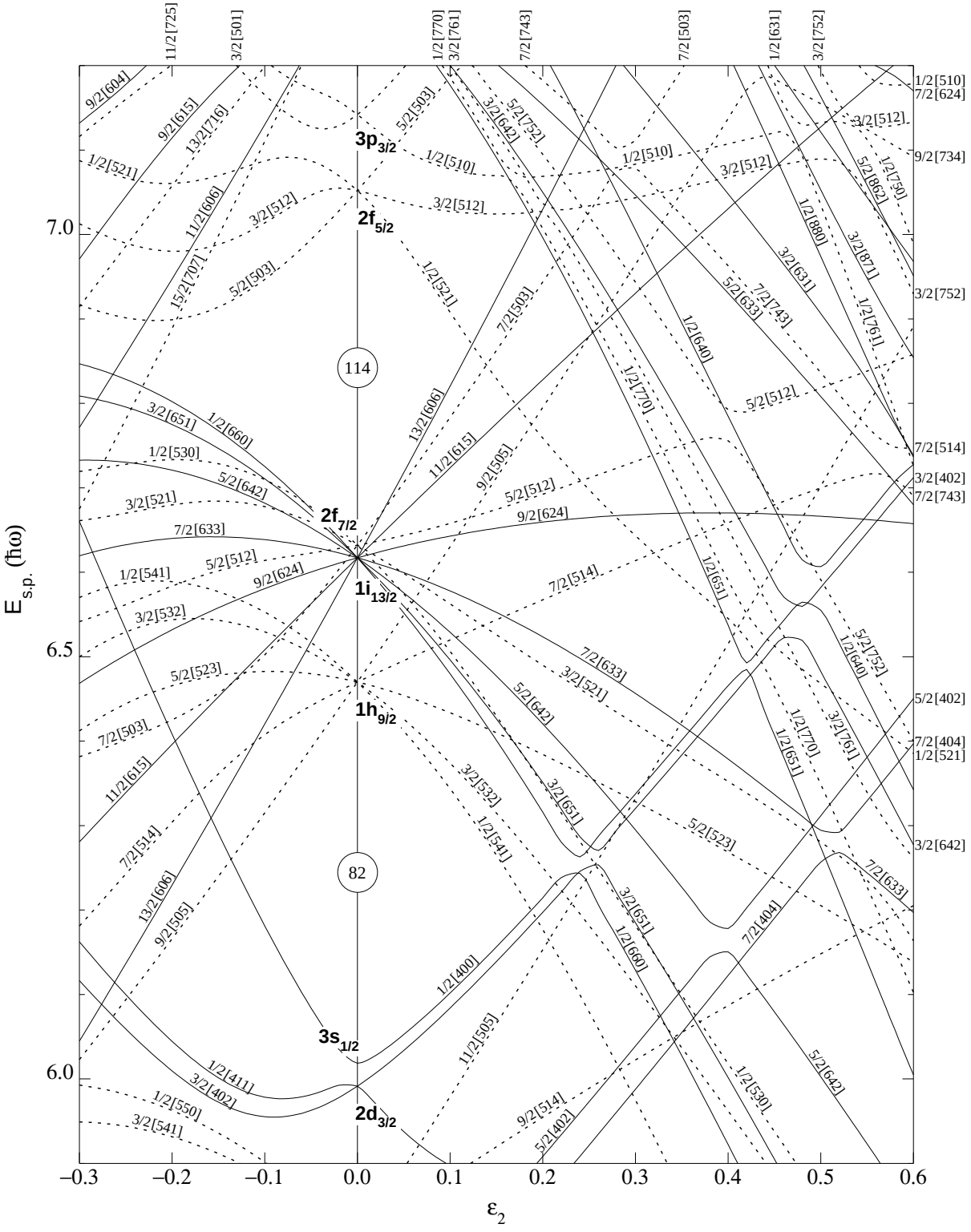

Figure 2.7: Nilsson diagram for protons, Z $\geq$ 82 [Fir97].

Chapter 3

Nuclear Moments

3.1 Magnetic Moment

The magnetic moment is a quantity that represents the magnitude and orientation of a magnetic field of a nucleus. As is the nature of the work presented, we will discuss theory based on closed shell ± 1 nucleon nuclei and should be assumed unless stated otherwise. We will also use the standard unit for magnetic moments, the nuclear magneton $\mu_N = \frac{e\hbar}{2m_\pi}$. Where e is the elementary charge, $\hbar$ is the reduced Planck's constant and m_π is the mass of the proton.

3.1.1 Magnetic Dipole

The magnetic moment of nuclei arises from the induction of magnetic fields due to the orbting charged particles (protons π) and the intrinsic spin $s = \frac{1}{2}$ of the nucleons (protons π and neutrons ν) in the nucleus. The strength of the orbital magnetic field will be proportional to the orbital angular momentum l of the valence proton.

The bare proton and neutron orbital and spin gyromagnetic factors are [NIS19]:

$$g_l^\pi = \mu_N, \quad g_l^\nu = 0 \ . \tag{3.1}$$

$$g_s^\pi = +5.586\mu_N, \quad g_s^\nu = -3.826\mu_N \ . \tag{3.2}$$

Following from this, we get the single-particle magnetic dipole moment operator:

$$\hat{\mu} = g_l^\pi \cdot \hat{l}_p + g_s^\nu \cdot \hat{s}_n + g_s^\pi \cdot \hat{s}_p \ , \tag{3.3}$$

where $\hat{l}_p$ is the proton orbital angular momentum operator, $\hat{s}_n$ and $\hat{s}_p$ are the neutron and proton spin operators respectively and the neutron orbital contribution excluded due to $g_l^\nu = 0$.

Now if we wish to find the value of the magnetic moment, we must apply this operator to the state with total spin I and projection m in which we are studying. As only the projection onto an axis can be measured, we use the standard quantization axis and can find the z-component of the magnetic moment or the magnetic dipole moment μ_z. Therefore the expectation value of $\hat{\mu}_z$ is the magnetic dipole moment μ:

$$\mu(I) = \langle I, m_{(m=I)} | \hat{\mu}_z | I, m_{(m=I)} \rangle \ . \tag{3.4}$$

In the single particle picture of a doubly magic core with a valance nucleon, with total angular momentum j around a stable core, we have the following relations that allow for the calculation of the magnetic dipole moment [Ney03]:

Proton:

$$\mu(j) = \begin{cases} j - \frac{1}{2} + \mu^{\pi} & \text{for} \quad j = l + \frac{1}{2} \\ (\frac{j}{j+1})(j + \frac{3}{2} - \mu^{\pi}) & \text{for} \quad j = l - \frac{1}{2} \ . \end{cases} \tag{3.5}$$

Neutron:

$$\mu(j) = \begin{cases} \mu^{\nu} & \text{for} \quad j = l + \frac{1}{2} \\ -(\frac{j}{j+1})\mu^{\nu} & \text{for} \quad j = l - \frac{1}{2} \ . \end{cases} \tag{3.6}$$

Here we use the free proton and neutron moments, $\mu^{\pi} = +2.793$ and $\mu^{\nu} = -1.913$.

The values calculated for $j = l \pm \frac{1}{2}$ of each nucleon, are the so called Schmidt moments and/or Schmidt limits [Sch37]. These are, to an extent, the limits in which most dipole moments of closed shell ± 1 nucleon nuclei fall between. This can be seen in Figure (3.1).

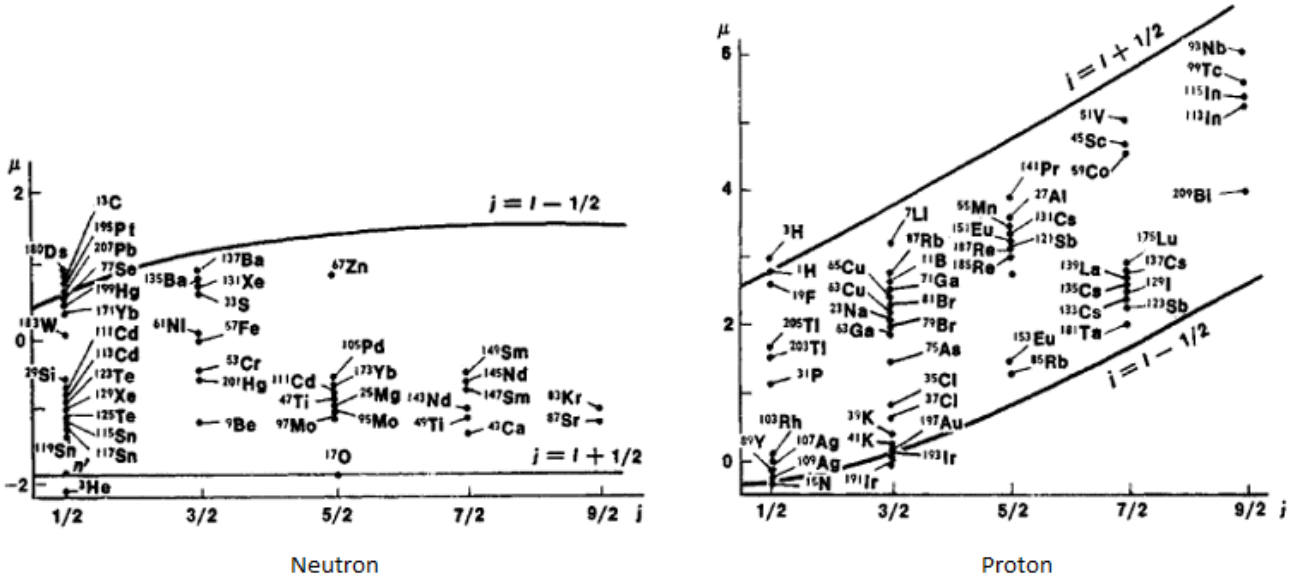

Figure 3.1: Diagram showing the Schmidt limits of dipole moments of closed shell ± 1 nucleon nuclei [McG05].

In our case where the total angular momentum $\hat{I} = \sum_{i=\nu,\pi}(\hat{l}_i + \hat{s}_i)$ of the system is conserved, it is possible to subtract the total angular momentum I_{μ_N} from the spectroscopic magnetic dipole moments of odd-Z nuclei only. This allows for us to define a spin magnetic dipole moment μ^s and therefore we can compare odd-Z and odd-N dipole moments in an identical manner:

$$\mu^s_{oddZ} \equiv \langle\hat{\mu}\rangle - I_{\mu_N} = g_l^{\nu\prime} \cdot \langle\hat{l}_n\rangle + g_s^{\nu\prime} \cdot \langle\hat{s}_n\rangle + g_s^{\pi\prime} \cdot \langle\hat{s}_p\rangle, \tag{3.7}$$

$$\mu^s_{oddN} \equiv \langle\hat{\mu}\rangle = g_l^{\pi} \cdot \langle\hat{l}_p\rangle + g_s^{\nu} \cdot \langle\hat{s}_n\rangle + g_s^{\pi} \cdot \langle\hat{s}_p\rangle. \tag{3.8}$$

where $\langle\rangle$ represents the standard matrix elements and:

$$g_l^{\nu\prime} = -\mu_N, \quad g_s^{\nu\prime} = -4.4826\mu_N, \quad g_s^{\pi\prime} = +4.586\mu_N. \tag{3.9}$$

3.2 Electric Moment

The electric quadrupole moment is a measure of the deviation of charge distribution from sphericity and the standard units are barns $b = 10^{-28}\mathrm{m}^2$.

3.2.1 Electric Quadrupole

The electric quadrupole moment is a quantity that is used to describe the shape of the nuclear charge distribution of the atomic nucleus. In many cases, this shape is not spherical and appears to be ellipsoidal, hence we introduce the parameter Q to represent the deviation from a spherical shape. Here we define the classical electric quadrupole moment operator:

$$\hat{Q} = e\sum_{i=1}^{Z}(3z_i^2 - r_i^2)\ , \tag{3.10}$$

where e is the usual electric charge, Z is the total number of protons (proton number) and z and r are the Cartesian coordinate position of the i^{th} nucleon.

Similar to the case for the magnetic dipole moment, we can calculate the spectroscopic electric quadrupole moment Q_s by finding the expectation value of the $\hat{Q}_z$ and applying the Wigner-Eckart theorem [dT63] (shown in Appendix A):

$$Q_s(I) = \langle I, m_{(m=I)}|\hat{Q}_z|I, m_{(m=I)}\rangle = \sqrt{\frac{I(2I-1)}{(2I+1)(2I+3)(I+1)}}\langle I||\hat{Q}_z||I\rangle, \tag{3.11}$$

where $\langle I||\hat{Q}_z||I\rangle$ is the electric quadrupole reduced matrix element.

From this, it is easy to see that for states with $I = \frac{1}{2}$ the spectroscopic quadrupole moment will be zero.

Now that we have formalism for the measured spectroscopic moment Q_s, we can include the theoretical intrinsic moment Q_0. These two are related by the following, on the condition that we assume that the deformation is large and axially symmetric and we have a defined orientation of the total spin [Ney03]:

$$Q_s = \frac{3K^2 - I(I+1)}{(I+1)(2I+3)} Q_0 \ , \tag{3.12}$$

$$Q_0 = \langle K|\hat{Q}|K\rangle \ , \tag{3.13}$$

where K is the projection of the total spin I onto the z symmetry axis and $|K\rangle$ is the intrinsic state determined from the Hartree-Fock method in Chapter 5.

Therefore, a non-zero value for the quadrupole moment indicates deformation. If Q_0 is negative the shape is oblate and if Q_0 is positive the shape is prolate, shown in Figure (3.2) where the vertical axis represents the z symmetry axis.

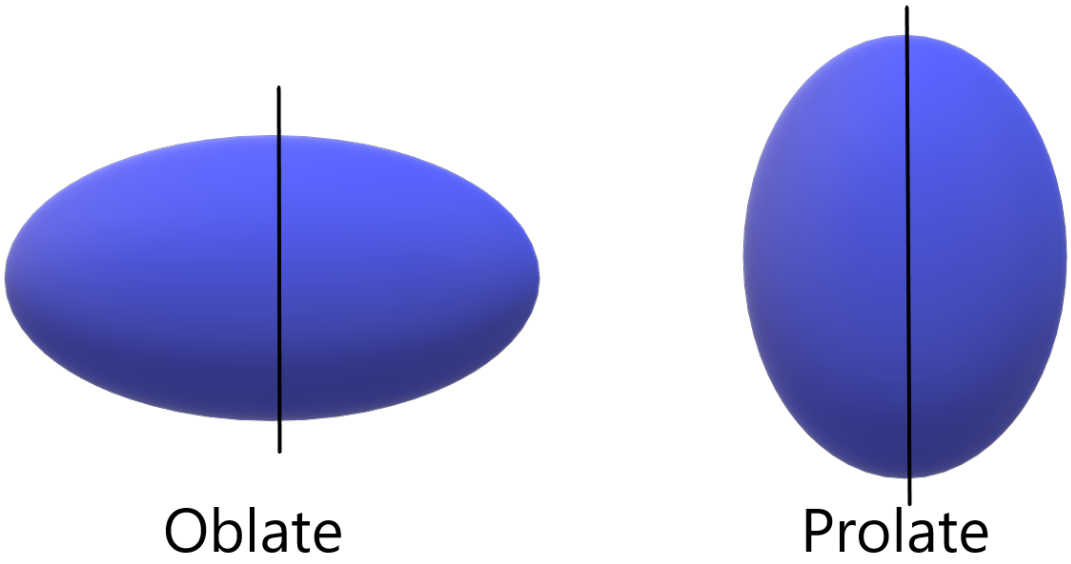

Figure 3.2: Diagram showing basic examples of oblate and prolate quadrupole deformed nuclei with respect to the z symmetry axis.

Chapter 4

Density Functional Theory

Density functional theory (DFT) is a computational modelling method whose basis stems from the variational principle and that uses observables as variational parameters such as the one-body densities as degrees of freedom. The principle of density functional theory is simply the constrainted minimisation of an observable, followed by a minimisation in function of the constraint. DFT is a tool which we can apply across the whole nuclear landscape for the study of nuclear structure.

We first begin with the definition of a functional. A functional is simply defined as a function of a function, which mathematically means that it maps a function into a number.

4.1 Variational Principle

The variational principle states that the ground-state energy E_0 of a system will be less than or equal to the expectation value of the Hamiltonian $\hat{H}$ using a normalised trial wavefunction Ψ:

$$E_0 \leq \langle \Psi | \hat{H} | \Psi \rangle \ . \tag{4.1}$$

By varying the wavefunction Ψ until we find the minimum for the expectation value of the Hamiltonian $\hat{H}$, we can then assume that an approximation of the ground-state energy E_0 and wavefunction Ψ_0 has been found:

$$E_0 = \langle \Psi_0 | \hat{H} | \Psi_0 \rangle \ . \tag{4.2}$$

4.2 Constrainted Variation

We are able to find the energy E of a system as a function of a select observable Q. This is done by the means of a constrainted variation.

First we take a set of parameters $\vec{p}$ such that they parameterise the whole Hilbert space $|\Psi(\vec{p})\rangle$. Hence we can define:

$$E(\vec{p}) = \langle\Psi(\vec{p})|\hat{H}|\Psi(\vec{p})\rangle \ , \tag{4.3}$$

$$Q(\vec{p}) = \langle\Psi(\vec{p})|\hat{Q}|\Psi(\vec{p})\rangle \ . \tag{4.4}$$

We then want to minimise the energy under a constraint given that the observable has a specific value. This can be done through the minimisation of the Routhian $\hat{R}$ [Dob16]:

$$\hat{R} = \hat{H} - \lambda\hat{Q} \ , \tag{4.5}$$

where λ is a constant called a Lagrange multiplier.

The minimisation of the Routhian is done by solving the derivative of the Routhian with respect to the parameters equal to zero:

$$\frac{\partial\hat{R}}{\partial\vec{p}} = \vec{\nabla}E - \lambda\vec{\nabla}Q = 0 \ . \tag{4.6}$$

From this, we can solve for all λ and obtain $\vec{p}(\lambda)$ and therefore we can redefine the energy and observable:

$$E(\vec{p}(\lambda)) = E(\lambda), \quad Q(\vec{p}(\lambda)) = Q(\lambda) \ . \tag{4.7}$$

Hence we can get the energy as a function of the observable $E(Q)$, now a functional, and find the ground-state energy E_0 and value of the observable Q_0 by solving the following:

$$\frac{\partial}{\partial Q}E(Q) = 0 \ . \tag{4.8}$$

There are multiple observables that can be chosen and hence will have their own specific representations in DFT due to the forms of the observables. This could be multiple observables used together or the observables are defined by a function and therefore complicating the calculations.

An example is that of the density ρ of spin σ $\frac{1}{2}$ and isospin τ $\frac{1}{2}$ particles [Dob16]:

$$E = E(\hat{\rho}(\vec{r};\sigma\tau,\sigma'\tau')) \Rightarrow \delta\left(\hat{H} + \sum_{\sigma\tau,\sigma'\tau'}\int \mathrm{d}\vec{r}\, U(\vec{r};\sigma'\tau',\sigma\tau)\hat{\rho}(\vec{r};\sigma\tau,\sigma'\tau')\right) = 0\ . \tag{4.9}$$

4.3 The Kohn-Sham Method

We can now discuss a method developed by Walter Kohn and Lu Jeu Sham in 1965 [KS65]. They propsed that the density can be represented by specific orbitals ϕ for the system. Their method is essentially the same as that of Hartree-Fock discussed in Chapter 5, however the Kohn-Sham method is solved using a fixed external potential built using a functional and the Hartree-Fock method uses a potential built with two-body interactions [Dob16].

We first consider the many-body Kohn-Sham Hamiltonian $\hat{H}_{KS}$:

$$\hat{H}_{KS} = \sum_{i=1}^{A}\hat{h}_{KS,i} = \int \mathrm{d}r\left[\left(\frac{\hbar^2}{2m} + M_{KS}(\vec{r})\right)\hat{\tau}(\vec{r}) + U_{KS}(\vec{r})\hat{\rho}_{KS}(\vec{r})\right]\ , \tag{4.10}$$

where $\hat{h}_{KS}$ is the one-body Kohn-Sham Hamiltonian:

$$\hat{h}_{KS} = -\nabla\left(\frac{\hbar^2}{2m} + M_{KS}(\vec{r})\right)\cdot\nabla + U_{KS}(\vec{r})\ . \tag{4.11}$$

It is known that the eigenstates of the one-body Kohn-Sham Hamiltonian are the specific orbitals of the system and hence:

$$\hat{h}_{KS}\phi_h^{KS}(\vec{r}) = \epsilon_h^{KS}\phi_h^{KS}(\vec{r})\ , \tag{4.12}$$

where ϵ_h^{KS} are the Kohn-Sham eigenenergies and $\phi_h^{KS}(\vec{r})$ are the Kohn-Sham orbitals.

From Equation (4.10), $\rho_{KS}(\vec{r})$ is the particle density and $\tau_{KS}(\vec{r})$ is the kinetic density defined as:

$$\rho_{KS}(\vec{r}) = \sum_{h=1}^{A}\phi_h^{KS}(\vec{r})\phi_h^{KS*}(\vec{r})\ , \tag{4.13}$$

$$\tau_{KS}(\vec{r}) = \sum_{h=1}^{A}\left(\nabla\phi_h^{KS}(\vec{r})\right)\cdot\left(\nabla\phi_h^{KS*}(\vec{r})\right)\ , \tag{4.14}$$

and therefore, we can define $M_{KS}(\vec{r})$ the Kohn-Sham mass function and $U_{KS}(\vec{r})$ the Kohn-Sham potential:

$$M_{KS}(\vec{r}) = \frac{\delta V[\rho,\tau]}{\delta\tau(\vec{r})}, \quad U_{KS}(\vec{r}) = \frac{\delta V[\rho,\tau]}{\delta\rho(\vec{r})} \ . \tag{4.15}$$

Finally, we are able to get the total energy, known as the Kohn-Sham energy E_{KS} defined as:

$$E_{KS}[\rho_{KS},\tau_{KS}] = \int \mathrm{d}r \left[\left(\frac{\hbar^2}{2m} + M_{KS}(\vec{r})\right)\tau_{KS}(\vec{r}) + U_{KS}(\vec{r})\rho_{KS}(\vec{r})\right] \ . \tag{4.16}$$

In order to calculate the energy we must solve the Kohn-Sham equations by means of a self-consistent iterative process:

1. Start with a sensible approximation for the potentials $M_{KS}(\vec{r})$ and $U_{KS}(\vec{r})$.
2. Diagonalise the one-body Kohn-Sham Hamiltonian $\hat{h}_{KS}$ to get the Kohn-Sham orbitals $\phi_h^{KS}(\vec{r})$.
3. Occupy the orbitals with particles from the lowest energy state to the Fermi level.
4. Then calculate the Kohn-Sham densities, $\rho_{KS}(\vec{r})$ and $\tau_{KS}(\vec{r})$, and Kohn-Sham potentials, $M_{KS}(\vec{r})$ and $U_{KS}(\vec{r})$.
5. Recycle the new densities and potentials back into the process until convergence is achieved.

Chapter 5

Hartree-Fock Method

The Hartee-Fock (HF) method is a method used to approximate the ground state wavefunction and energy of a stationary, many-body quantum system.

5.1 Hartree-Fock Approximation

We need to begin with the general Hamiltonian in which only two-body interactions are considered in order to describe the nucleus in terms of its nucleons. The following is the mentioned Hamiltonian in second quantization form (detailed in Appendix B):

$$\hat{H} = \sum_{ij} t_{ij}\, \hat{a}_i^\dagger \hat{a}_j + \frac{1}{4} \sum_{ijkl} \bar{v}_{ijkl}\, \hat{a}_i^\dagger \hat{a}_j^\dagger \hat{a}_l \hat{a}_k \ , \tag{5.1}$$

where t_{ij} is the usual kinetic energy, $\hat{a}^\dagger$ and $\hat{a}$ are the creation and annihilation operators respectively and v_{ijkl} are the matrix elements of the nucleon-nucleon interaction. The indices i, j, k, l are the labels used to represent the single-particle states.

In the Hartree-Fock method, we work under the assumption that the nuclear wavefunction can be expressed as a product of single-particle states [GM96]:

$$\begin{aligned} |\Psi\rangle &= \hat{a}_1^\dagger \ldots \hat{a}_i^\dagger |0\rangle \\ &= \prod_{i=1}^{A} \hat{a}_i^\dagger |0\rangle \ . \end{aligned} \tag{5.2}$$

This is commonly known as a Slater determinant and can also have the following form, which we shall call the Hartree-Fock wavefunction:

$$|\Psi\rangle = \Phi_i(\mathbf{r}_1 \ldots \mathbf{r}_A) = \begin{vmatrix} \phi_1(\mathbf{r}_1) & \phi_1(\mathbf{r}_2) & \ldots & \ldots & \phi_1(\mathbf{r}_A) \\ \phi_2(\mathbf{r}_1) & \phi_2(\mathbf{r}_2) & \ldots & \ldots & \phi_2(\mathbf{r}_A) \\ \ldots & \ldots & \ldots & \ldots & \ldots \\ \ldots & \ldots & \ldots & \ldots & \ldots \\ \phi_A(\mathbf{r}_1) & \phi_A(\mathbf{r}_2) & \ldots & \ldots & \phi_A(\mathbf{r}_A) \end{vmatrix} , \tag{5.3}$$

where $i = 1, \ldots, A$, and the single-particle wavefunctions, ϕ_i, are to be determined by the variational principle [RS04].

5.2 Hartree-Fock Equations

By calculating the Hartree-Fock energy, we are able to introduce an average single-particle potential used to deal with long-range effects of the nuclear interaction and a single-particle density matrix to simplify the method.

By using Wick's theorem [Wic50] (shown in Appendix C), we are able to calculate the Hartree-Fock energy E_{HF} given by the following expression:

$$E_{HF} = \sum_{ij} t_{ij}\rho_{ji} + \frac{1}{2}\sum_{ijkl} \bar{v}_{ijkl}\rho_{ki}\rho_{lj} \ . \tag{5.4}$$

From this we can define the density matrix ρ (in second quantization) and the Hartree-Fock potential h:

$$\rho_{ij} = \langle\Psi|\hat{a}_j^\dagger \hat{a}_i|\Psi\rangle \ , \tag{5.5}$$

$$h_{ij} = t_{ij} + \Gamma_{ij} \ , \tag{5.6}$$

where the self-consistent field Γ is:

$$\Gamma_{ij} = \sum_{kl} \bar{v}_{iljk}\rho_{kl} \ . \tag{5.7}$$

Now we can express the Hartree-Fock energy in the simple form:

$$E_{HF} = \mathrm{Tr}\ t\rho + \frac{1}{2}\mathrm{Tr}\ \Gamma\rho \ , \tag{5.8}$$

where Tr is the trace of a matrix and owing to the fact that $\rho^2 = \rho$ and $\mathrm{Tr}\rho = A$, due to the density and Hartree-Fock potential being diagonal [RS04].

This then leads to the solving of the Hartree-Fock equations by means of a self-consistent iterative process:

1. Start with an intitial set of trial wavefunctions.
2. Construct the density and find the Hartree-Fock potential.
3. Solve the Hartree-Fock equations to generate new states.
4. Recycle the new wavefunctions into the process until convergence is achieved.

Convergence is achieved in the process by if the new wavefunctions fed into the method no longer change. Figure (5.1) shows a basic schematic of the process.

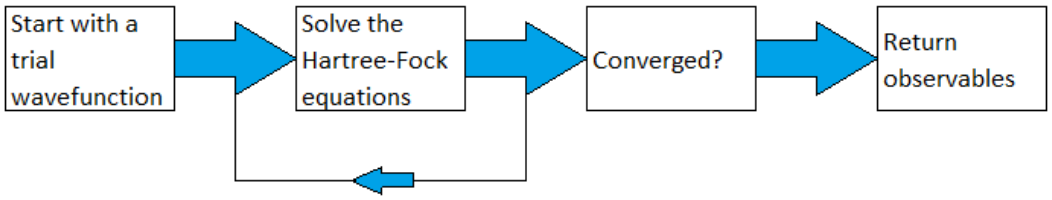

Figure 5.1: Basic schematic of the Hartree-Fock iterative process for solving the Hartree-Fock equations and calculating the wavefunctions.

Chapter 6

Energy Density Functionals

We begin by introducing the equipment required to build an energy functional. The functional can be build from the basic single-particle density matrix $\hat{\rho}$ with the spatial $\boldsymbol{r}$, spin σ and isospin τ coordinates of the wavefunction [Ben02]:

$$\begin{aligned}\hat{\rho} = \rho(\mathbf{r},\sigma,\tau,\mathbf{r}',\sigma',\tau') \;\; = \;\; & \tfrac{1}{4}\Big[\rho_{00}(\mathbf{r},\mathbf{r}')\delta_{\sigma\sigma'}\delta_{\tau\tau'} + \boldsymbol{s}_{00}(\mathbf{r},\mathbf{r}')\cdot\boldsymbol{\sigma}_{\sigma\sigma'}\delta_{\tau\tau'} \\ & +\delta_{\sigma\sigma'}\sum_{t_3=-1}^{+1}\rho_{1t_3}(\mathbf{r},\mathbf{r}')\tau^{t_3}_{\tau\tau'} \\ & +\sum_{t_3=-1}^{+1}\boldsymbol{s}_{1t_3}\cdot\boldsymbol{\sigma}_{\sigma\sigma'}\tau^{t_3}_{\tau\tau'}\Big] \;,\end{aligned} \tag{6.1}$$

where $\boldsymbol{\sigma}_{\sigma\sigma'}$ and $\tau^{t_3}_{\tau\tau'}$ are the matrix elements of the spin and isospin Pauli matrices respectively.

Therefore we can now define the local density ρ, the spin density $\boldsymbol{s}$, the kinetic density τ, the kinetic spin density $\boldsymbol{T}$, the current $\boldsymbol{j}$ and the spin-orbit tensor $\overleftrightarrow{J}$ [Ben02]:

$$\rho_{tt_3}(\mathbf{r}) = \rho_{tt_3}(\mathbf{r},\mathbf{r}) \;, \tag{6.2}$$

$$\boldsymbol{s}_{tt_3}(\mathbf{r}) = \boldsymbol{s}_{tt_3}(\mathbf{r},\mathbf{r}) \;, \tag{6.3}$$

$$\tau_{tt_3}(\mathbf{r}) = \nabla\cdot\nabla'\rho_{tt_3}(\mathbf{r},\mathbf{r}')\mid_{\mathbf{r}=\mathbf{r}'} \;, \tag{6.4}$$

$$\boldsymbol{T}_{tt_3}(\mathbf{r}) = \nabla\cdot\nabla'\boldsymbol{s}_{tt_3}(\mathbf{r},\mathbf{r}')\mid_{\mathbf{r}=\mathbf{r}'} \;, \tag{6.5}$$

$$\boldsymbol{j}_{tt_3}(\mathbf{r}) = -\frac{i}{2}(\nabla-\nabla')\rho_{tt_3}(\mathbf{r},\mathbf{r}')\mid_{\mathbf{r}=\mathbf{r}'} \;, \tag{6.6}$$

$$\overleftrightarrow{J}_{tt_3,ij}(\mathbf{r}) = -\frac{i}{2}(\nabla - \nabla')_i \boldsymbol{s}_{tt_3,j}(\mathbf{r},\mathbf{r}')\mid_{\mathbf{r}=\mathbf{r}'} \ . \tag{6.7}$$

6.1 Skyrme Interaction

The Skyrme interaction is an effective interaction first proposed in 1956 by Tony Hilton Royle Skyrme [Sky56]. The interaction was originally designed to be used in Hartree-Fock calulations, however it is possible to be used with the Kohn-Sham method due to both methods being similar.

The interaction can be written as a potential Υ consisting of two parts. First being a two-body term υ_{ij} and the second being a three-body term υ_{ijk} [VB72]:

$$\Upsilon = \sum_{i<j} \upsilon_{ij}^{(2)} + \sum_{i<j<k} \upsilon_{ijk}^{(3)} \ , \tag{6.8}$$

These terms can be written in the following form using notation from [Ben02]:

$$\begin{aligned} \upsilon_{Skyrme}(\mathbf{r}_1,\mathbf{r}_2) \ = \ & t_0(1+x_0\hat{P}_\sigma)\delta(\mathbf{r}_1-\mathbf{r}_2) + \tfrac{1}{2}t_1(1+x_1\hat{P}_\sigma) \\ & \times\left[\hat{\mathbf{k}'}^2\delta(\mathbf{r}_1'-\mathbf{r}_2') + \delta(\mathbf{r}_1-\mathbf{r}_2)\hat{\mathbf{k}}^2\right] \\ & + t_2(1+x_2\hat{P}_\sigma)\hat{\mathbf{k}'}\cdot\delta(\mathbf{r}_1-\mathbf{r}_2)\hat{\mathbf{k}} \\ & + \tfrac{1}{6}t_3(1+x_3\hat{P}_\sigma)\delta(\mathbf{r}_1-\mathbf{r}_2)\rho^\alpha\left(\tfrac{\mathbf{r}_1+\mathbf{r}_2}{2}\right) \\ & + iW_0(\hat{\boldsymbol{\sigma}}_1+\hat{\boldsymbol{\sigma}}_2)\cdot\hat{\mathbf{k}'}\times\delta(\mathbf{r}_1-\mathbf{r}_2)\hat{\mathbf{k}} \ , \end{aligned} \tag{6.9}$$

where $\hat{P}_\sigma = \frac{1}{2}(1+\hat{\boldsymbol{\sigma}}_1\cdot\hat{\boldsymbol{\sigma}}_2)$ is the spin-exchange operator, $\frac{1}{6}t_3(1+x_3\hat{P}_\sigma)\delta(\mathbf{r}_1-\mathbf{r}_2)\rho^\alpha\left(\frac{\mathbf{r}_1+\mathbf{r}_2}{2}\right)$ represents the three-body term reduced to a two-body density-dependent interaction, $\hat{\mathbf{k}} = -(\frac{i}{2})(\nabla_1-\nabla_2)$ is the operator acting to the right and $\hat{\mathbf{k}'} = (\frac{i}{2})(\nabla_1'-\nabla_2')$ is the operator acting to the left.

6.2 Skyrme Functional

The Skyrme energy functional $\mathcal{E}$ is given by the three-dimensional integral of the energy density $\mathcal{H}$ [DD95]:

$$\mathcal{E} = \int \mathrm{d}^3\mathbf{r}\mathcal{H}(\mathbf{r}) \ . \tag{6.10}$$

The energy density can now be broken down to three parts; a kinetic part $\mathcal{H}_{kinetic}$, a Skyrme part $\mathcal{H}_{Skyrme}$ which is further broken down into time-even and time-odd terms, and an electro-

magnetic part $\mathcal{H}_{em}$ which uses the coulomb interaction:

$$\mathcal{H}_{Skyrme} = \sum_{t=0,1} \sum_{t_3=-t}^{t} (\mathcal{H}^{even}_{tt_3} + \mathcal{H}^{odd}_{tt_3}) \ . \tag{6.11}$$

Using definitions and notation from [DD95], we get the following for the Skyrme energy functional (all coupling constants C are shown in Appendix D):

$$\begin{aligned} \mathcal{H}_{Skyrme} \ = \ & \sum_{t=0,1} \sum_{t_3=-t}^{t} \Big[C^{\rho}_{t} \rho^2_{tt_3} + C^{s}_{t} \boldsymbol{s}^2_{tt_3} + C^{\Delta\rho}_{t} \rho_{tt_3} \Delta\rho_{tt_3} \\ & + C^{\Delta s}_{t} \boldsymbol{s}_{tt_3} \cdot \Delta \boldsymbol{s}_{tt_3} + C^{\tau}_{t} (\rho_{tt_3} \tau_{tt_3} - \boldsymbol{j}^2_{tt_3}) \\ & + C^{T}_{t} (\boldsymbol{s}_{tt_3} \cdot \boldsymbol{T}_{tt_3} - \overleftrightarrow{J}^2_{tt_3}) + C^{\nabla J}_{t} (\rho_{tt_3} \nabla \cdot \mathbf{J}_{tt_3} + \boldsymbol{s}_{tt_3} \cdot \nabla \times \boldsymbol{j}_{tt_3}) \\ & + C^{\nabla s}_{t} (\nabla \cdot \boldsymbol{s}_{tt_3})^2 \Big] \ . \end{aligned} \tag{6.12}$$

6.3 Skyrme Parameterisations

There are multiple parameterisations that can be used for the functionals, with them being determined by fitting or constraining parameters to reproduce certain observables and/or nuclear properties. We briefly mention each parameterisation used in this work and how they differ from one another. It should be mentioned that the UNEDF1, SLy4 and SkO′ functionals have all been fitted to ground state masses, radii and nuclear matter properties.

6.3.1 UNEDF1

The UNEDF1 is a Skyrme parameterisation which was developed by mainly removing centre-of-mass corrections in the functional which allowed for the global description of multiple nuclear properties, with the main being the ability to reproduce masses, separation energies and the empirical fission barriers in the actinide region [Kor12].

6.3.2 SLy4

The SLy4 is a Skyrme parameterisation which was developed by corrections to the centre-of-mass correlations and the spin-orbit interaction. This allowed for the parameterisation to reproduce the binding energy of doubly magic nuclei and the rms radii for each [Cha98].

6.3.3 SkO′

The SkO′ is a Skyrme parameterisation which was developed by changes done to the effective interaction. This has allowed the parameterisation to reproduce total binding energies and nuclear densities for nuclei, and by constraining certain observables can produce single-particle energies for the magic nuclei [Rei99].

6.4 Additional Functionals

There are multiple other functionals that use different methods and parameterisations. For the work presented in this thesis, we used two additional functionals for some variation with our research.

6.4.1 Gogny - D1S

The Gogny is a different functional to the Skyrme due to its construction, the difference being that the two-body part is explicitly finite-ranged and has the form of a Gaussian [BGG91]. This specific Gogny parameterisation for the D1S interaction has the following form:

$$\begin{aligned} \upsilon_{12}^{\mathrm{D1S}} \;=\; & \sum_{j=1}^{2} \exp\left(-\tfrac{(\mathbf{r}_1-\mathbf{r}_2)^2}{\mu_j^2}\right) \\ & \times (W_j + B_j P_\sigma - H_j P_\tau - M_j P_\sigma P_\tau) \\ & + t_3(1+x_0 P_\sigma)\delta(\mathbf{r}_1-\mathbf{r}_2)\left[\rho\left(\tfrac{\mathbf{r}_1+\mathbf{r}_2}{2}\right)\right]^{\alpha} \\ & + iW_{LS}\nabla_{12}\delta(\mathbf{r}_1-\mathbf{r}_2)\times\nabla_{12}\cdot(\boldsymbol{\sigma}_1+\boldsymbol{\sigma}_2) \\ & + (1+2\tau_{1z})(1+2\tau_{2z})\tfrac{e^2}{|\mathbf{r}_1-\mathbf{r}_2|}\ . \end{aligned} \tag{6.13}$$

6.4.2 Regularized - N^{3}LO

The regularized N^{3}LO is another functional different from Skyrme and Gogny, where it uses finite-range pseudopotentials to produce the functional. This functional uses the spin-orbit and density to provide good values of the binding energies and radii of nuclei [Ben20b].

6.5 Landau Parameters

The Landau Parameters are constants that govern the values of other coupling constants in the Skyrme functional. All Landau parameters are dependent on a normalization factor N_0 defined

as the level density at the Fermi surface of the system and takes the form:

$$\frac{1}{N_0} = \frac{\pi^2\hbar^2}{2m^* k_f} \approx 150\frac{m}{m^*}\text{MeV fm}^3 \ , \tag{6.14}$$

where m^* is the effective mass.

There are eight total Landau parameters, however for our research only two were of any significance. These two Landau parameters are constants that govern the isoscalar g_0 and isovector g_0' time-odd, spin-spin channels of the calculations that were performed. These parameters specify certain values used to calculate time-odd coupling constants in which are used to calculate densities and potentials and are defined as follows:

$$g_0 = N_0(2C_0^s + 2C_0^T\beta\rho_{00}^{2/3}) \ , \tag{6.15}$$

$$g_0' = N_0(2C_1^s + 2C_1^T\beta\rho_{00}^{2/3}) \ . \tag{6.16}$$

Chapter 7

Symmetry Restoration

Not discussed in previous Chapters, the method which we use to get solutions may break certain symmetries of the system. We can however choose what symmetries we wish to break, or impose, for desired outcomes and we have the methods to restore these symmetries when needed. A simple way of thinking about the wave functions in this sense of symmetries is; if we are referring to the intrinsic reference frame, this can be interpreted as the symmetries have been broken but not restored and if we are referring to the laboratory/spectroscopic reference frame, this can be intepreted as the symmetries have been broken and restored [She21].

7.1 Relevant Symmetries

7.1.1 Parity, Signature and Time-reversal

Parity is simply the operation of inverting the spacial coordinates of the polar vector such as position $\boldsymbol{r}$ and momentum $\boldsymbol{p}$, therefore acting on each with the parity operator $\hat{P}$ results in:

$$\hat{P}\boldsymbol{r} = -\boldsymbol{r}, \quad \hat{P}\boldsymbol{p} = -\boldsymbol{p}\ . \tag{7.1}$$

The parity operator is its own inverse ($\hat{P}^2 = 1$), easily seen by applying the operator twice and returning to the original coordinates, and therefore its eigenvalues π can only be the values ± 1.

Signature is defined as the rotation of a system with total angular momentum J about the axis perpendicular to the symmetry axis by π (180°). Similar to parity, applying the signature operature $\hat{R} = \exp(-i\pi J)$ twice will result in the system returning to its original orientation hence it is also its own inverse ($\hat{R}^2 = 1$). The eigenvalues r of this operator depend on the number of particles A in the system. If A is even, $r = \pm 1$, and if A is odd, $r = \pm i$.

Time-reversal reverses the time component of terms. This will only affect certain quantities such as momentum p. The time-reversal operator is defined as $\hat{T} = -i\hat{l}\hat{K}$, where $\hat{l}$ is the intrinsic angular momentum operator and $\hat{K}$ is the complex conjugate operator.

7.2 Restoration Methods

We can restore the symmetries broken by the calculation of the wave functions within our approach using two methods; variation-after-projection (VAP) or projection-after-variation (PAV).

7.2.1 Variation-after-projection (VAP)

The VAP method is one which minimises the projected energy of the symmetry restored wavefunction Φ [RS04]:

$$\delta \frac{\langle \Phi | H | \Phi \rangle}{\langle \Phi | \Phi \rangle} = \delta \frac{\langle \phi | \hat{P} H \hat{P} | \phi \rangle}{\langle \phi | \hat{P} \hat{P} | \phi \rangle} = 0 \ , \tag{7.2}$$

where $|\phi\rangle$ is the product wavefunction and the projection operator $\hat{P}$ is a combination of multiple projection operators.

7.2.2 Projection-after-variation (PAV)

The PAV method is one which minimises the energy of the product wavefunction $|\phi\rangle$, then the projection operators are applied to restore the symmetries [RS04]:

$$\delta \frac{\langle \phi | H | \phi \rangle}{\langle \phi | \phi \rangle} = 0 \ , \tag{7.3}$$

where we then apply the projection operator $\hat{P}$ to get the final wavefunction Φ:

$$|\Phi\rangle = \hat{P} |\phi\rangle \ . \tag{7.4}$$

Chapter 8

Methodology

In this section, we will detail the methods used in previous studies by past groups and the methods we have employed for our research presented in this thesis.

8.1 Previous Research Methods

As mentioned in Chapter 1, the groups that have previously studied nuclear moments will have their methods detailed and will be referred to as 'Borrajo and Egido', 'Péru et al', 'Bonneau et al', 'Li et al' and 'Co' et al' for convienience.

In all papers published by 'Borrajo and Egido' in the subject (exclusively Mg isotopes) [BE16] [BE17] [BE18a] [BE18b], they have used the Hartree-Fock-Bogoliubov (HFB) approach using the Gogny interaction with the D1S parameterisation. In their calculations, the symmetries they have conserved are parity, signature and time-reversal. They have also done their calculations using triaxial deformation and they have used blocking in order to get the correct spin and parity states. They have implemented the use of collective mixing by means of symmetry conserving configuration mixing (SCCM). This group also employs the use of angular momentum projection (AMP), in which they use the variation after projection (VAP) approach.

The 'Péru et al' group (exclusively Hg isotopes) [Pér21] used the Hartree-Fock-Bogoliubov (HFB) approach with the Gogny interaction implementing the D1M parameterisation. This group has conserved parity/inversion, signature and time-reversal symmetries and used axial deformation. This group has used a spin quenching factor (effective spin g-factor) of 0.75 in order to fit experimental data. They have also employed blocking of neutron states to try achieve the correct ground state of the nuclei. There has been no use of angular momentum projection, however they have used a correction to the magnetic moment which stems from their aim to include collectivity.

As for the 'Bonnaeu et al' group (various nuclei) [Bon12] [Bon15], their approach was to use the Hartree-Fock Bardeen-Cooper-Schrieffer model (BCS) with the Skyrme interaction using the SIII and SLyIII.0.8 parameterisations. They conserve parity/inversion, while breaking time-reversal and as a consequence, signature is broken too. They have used axial deformation in their calculations. Just like 'Péru et al', they have implemented the use of effective spin g-factors ranging from 0.7-0.9 in their calculations and have implemented blocking of the lowest K^{π} state above the even-even core. They have not performed any angular momentum projection (AMP) in their work.

In the papers by 'Li and Meng' (various nuclei) [WLM12] [LM18], they have used a more complex method which takes into consideration relativistic effects, the so called covariant density functional theory (CDFT) which we can consider as another type of functional. With this approach, they incorporate certain corrections such as meson exchange currents and 1st order (spin polarization effect) and 2nd order (quadrupole polarization effect) configuration mixing. This group has restricted themselves to spherical calculations as they state that these nuclei are "usually spherical".

In the paper by 'Co' et al' (various nuclei) [Co15], they used pure Hartree-Fock (HF) in their approach, however have opted to using a single-particle (s.p.) basis. They have imposed spherical symmetry on the systems, hence conserving parity, signature and time-reversal. They have not used any effective g-factors in their work and have relied on a residual interaction through the implementation of random phase approximation (RPA). They have also used corrections in their work in determining the magnetic moment, meson exchange currents.

8.2 Our Approach

In our work we use nuclear density functional theory (DFT) to determine the magnetic dipole μ and electric quadrupole Q moments of 32 nuclei, where the pure Hartree-Fock (HF) appraoch was used using the Skyrme (UNEDF1 [Kor12], SLy4 [Cha98] and SkO′ [Rei99]), Gogny (D1S [BGG91]) and regularized (N^3LO [Ben20b]) interaction, with emphasis on Skyrme using the UNEDF1 parameterisation and secondary focus on the SLy4 and SkO′ parameterisations. Within the calculations we used the Cartesian deformed harmonic-oscillator basis with the spherical basis of $N_0 = 16$ oscillator shells. We used pure HF for our calculations as the 32 nuclei we have chosen are one-particle and one-hole neighbours of 8 doubly magic nuclei (^{16}O, ^{40}Ca, ^{48}Ca, ^{56}Ni, ^{78}Ni, ^{100}Sn, ^{132}Sn and ^{208}Pb), therefore we need not worry about pairing contributions or collectivity. The time-reversal and signature symmetries were broken in our calculations, which induced polarisation effects, and we implemented angular momentum pro-

jection (AMP) to restore these symmetries with the projection-after-variation (PAV) approach. Relative to the doubly magic nuclei, configurations of odd-particle (odd-hole) nuclei were fixed by occupying (emptying) deformed substates that originated from a given spherical orbital and had the highest-positive (lowest-negative) value of Ω. The chosen single-particle occupations thus always corresponded to the maximally aligned total angular momenta, $\Omega = +I$. Such occupations yielded the oblate (prolate) self-consistent intrinsic shapes for odd-particle (odd-hole) $I > \frac{1}{2}$ nuclei and vice versa for $I = \frac{1}{2}$. The main aspect of the work was to study the dependance of the results on the isovector time-odd spin-spin Landau parameter g_0'. We also studied the dependance of the isoscalar time-odd spin-spin Landau parameter g_0, however this parameter proved to show no relevance in the calculations and was set to $g_0 = 0.4$ recommended from [Ben02].

The following table shows each group and their methods.

	Borrajo and Egido	**Pèru et al.**	**Bonneau et al.**	**Li and Meng**	**Cò et al.**	**Sassarini et al.**
Nuclei Region	Mg isotopes	Hg isotopes	A≈50, 100, 178, 236	A≈16, 40, 208	Doubly magic	All doubly magic
HF				✓	✓	✓
HF-BCS			✓			
HFB	✓	✓				
Single-particle Operator	✓	✓	✓	MEC	MEC	✓
Eff. Spin g-factor		✓	✓			
Core contribution	Microscopic	Model	Microscopic	Model	Model	Microscopic
Collective Mixing (BMF)	✓					
Blocking	✓	✓	✓	N/A	N/A	N/A
AMP	✓					✓
Skyrme			SIII, SLyIII.0.8			UNEDF1, SLy4, SkO′
Gogny	D1S	D1M			D1S, D1M	D1S
Regularized						N^3LO
Relativistic Lagrangian				✓		
HO Basis	Spherical	Deformed	Cylindrical	Spherical	Single-particle	Spherical
Oscillator Shells	8	19	13	not specified	N/A	16
Parity	✓	✓	✓	✓	✓	✓
Signature	✓	✓		✓	✓	
Time-reversal	✓	✓		✓	✓	
Spherical				✓	✓	
Axial		✓	✓			✓
Triaxial	✓					
Reference Frame	Intrinsic	Intrinsic	Intrinsic	Laboratory	Laboratory	Intrinsic

Table 8.1: Tabular comparison of the differences of work done by other groups and our own, detailing the methods and symmetries imposed.

Chapter 9

Results

9.1 Ground States

All the results for our calculations of the ground states of all nuclei studied are displayed in Table (9.1) for the magnetic dipole moments and in Table (9.2) for the electric quadrupole moments. In these tables we have included the Nilsson labels for each with the occupied orbitals and spin and parity of the level, the experimental data and the reference for each, all the results of our calculations for each functional and the average and RMS deviations for all the functionals. It should be noted that for ^{101}Sn and ^{47}K using the SkO$'$ parameterisation, we were unable to get converged solutions hence their values are missing from the tables. Also, the expected ground state for ^{131}Sn was the $2d_{3/2}$ state as seen in calculations from [Ben20a] and from the Nilsson plot Figure (2.3), however for our study we used the $1h_{11/2}$ state in accordance to available experimental data.

				Magnetic dipole moment μ (μ_N)							
Nuclide	I^π	$[Nn_z\Lambda]K$	orbital	EXP	Ref.	UNEDF1	SLy4	SkO′	D1S	N^{3}LO	Average
^{15}O	$\frac{1}{2}^-$	[101]1/2	$1p_{1/2}$	0.71951(12)*	[Sto05]	0.6366	0.6372	0.6384	0.6369	0.6352	0.6369(10)
^{17}O	$\frac{5}{2}^+$	[202]5/2	$1d_{5/2}$	−1.89379(9)*	[Sto05]	−1.9081	−1.9092	−1.9090	−1.9098	−1.9091	−1.9090(6)
^{15}N	$\frac{1}{2}^-$	[101]1/2	$1p_{1/2}$	−0.2830569(14)*	[Ant05]	−0.2632	−0.2638	−0.2651	−0.2632	−0.2616	−0.2634(12)
^{17}F	$\frac{5}{2}^+$	[202]5/2	$1d_{5/2}$	4.7223(12)*	[Sto05]	4.7878	4.7890	4.7881	4.7895	4.7889	4.7887(6))
^{39}Ca	$\frac{3}{2}^+$	[202]3/2	$1d_{3/2}$	1.02168(12)	[Sto05]	1.1465	1.1468	1.1476	1.1472	1.1469	1.1470(4)
^{41}Ca	$\frac{7}{2}^-$	[303]7/2	$1f_{7/2}$	−1.5942(7)	[Sto05]	−1.9088	−1.9099	−1.9098	−1.9098	−1.9098	−1.9096(4)
^{39}K	$\frac{3}{2}^+$	[202]3/2	$1d_{3/2}$	0.39147(3)	[Sto05]	0.1259	0.1256	0.1249	0.1251	0.1255	0.1254(4)
^{41}Sc	$\frac{7}{2}^-$	[303]7/2	$1f_{7/2}$	5.431(2)*	[Sto05]	5.7886	5.7897	5.7888	5.7896	5.7895	5.7892(5)
^{47}Ca	$\frac{7}{2}^-$	[303]7/2	$1f_{7/2}$	−1.4064(11)	[Gar15]	−1.4113	−1.3232	−1.2991	−1.4894	−1.4248	−1.39(7)
^{49}Ca	$\frac{3}{2}^-$	[301]3/2	$2p_{3/2}$	−1.3799(8)	[Gar15]	−1.6506	−1.6494	−1.6530	−1.7090	−1.6607	−1.66(2)
^{47}K	$\frac{1}{2}^+$	[220]1/2	$2s_{1/2}$	1.933(9)	[Sto05]	2.2040	2.0786	2.2958	2.4801	2.5769	2.33(18)
^{49}Sc	$\frac{7}{2}^-$	[303]7/2	$1f_{7/2}$	5.539(4)	[Bai22]	5.3409	5.4636	5.6621	5.6127	5.4734	5.51(11)
^{55}Ni	$\frac{7}{2}^-$	[303]7/2	$1f_{7/2}$	−0.98(3)*	[Ber09]	−1.1009	−1.0923	−1.0309	−1.3596	−1.1638	−1.15(11)
^{57}Ni	$\frac{3}{2}^-$	[301]3/2	$2p_{3/2}$	−0.7975(14)*	[Sto05]	−1.3267	−1.4371	−0.4178	−1.5227	−1.4261	−1.43(7)**
^{55}Co	$\frac{7}{2}^-$	[303]7/2	$1f_{7/2}$	4.822(3)*	[Sto05]	4.9296	4.8991	4.8016	5.1811	4.9969	4.96(13)
^{57}Cu	$\frac{3}{2}^-$	[301]3/2	$2p_{3/2}$			3.1759	3.2968	2.0319	3.4081	3.2944	3.29(8)**
^{77}Ni	$\frac{9}{2}^+$	[404]9/2	$1g_{9/2}$			−1.2069	−1.1768	−1.1414	−1.4322	−1.2563	−1.24(10)
^{79}Ni	$\frac{5}{2}^+$	[402]5/2	$2d_{5/2}$			−1.5128	−1.5542	−1.4924	−1.6529	−1.5754	−1.56(6)
^{77}Co	$\frac{7}{2}^-$	[303]7/2	$1f_{7/2}$			4.9185	4.9234	4.7569	5.1730	4.9936	4.95(13)
^{79}Cu	$\frac{3}{2}^-$	[301]3/2	$2p_{3/2}$			3.2102	3.3391	3.3742	3.4565	3.3927	3.35(8)
^{99}Sn	$\frac{9}{2}^+$	[404]9/2	$1g_{9/2}$			−1.2018	−1.1918	−1.1477	−1.4448	−1.2608	−1.25(10)
^{101}Sn	$\frac{5}{2}^+$	[402]5/2	$2d_{5/2}$			−1.4674	−1.4968		−1.5824	−1.4956	−1.51(4)**
^{99}In	$\frac{9}{2}^+$	[404]9/2	$1g_{9/2}$			6.0398	6.0097	5.9342	6.2765	6.1021	6.07(12)
^{101}Sb	$\frac{7}{2}^+$	[404]7/2	$1g_{7/2}$			2.2721	2.1716	2.1604	2.1313	2.1465	2.18(5)
^{131}Sn	$\frac{11}{2}^-$	[505]11/2	$1h_{11/2}$	−1.267(1)	[Yor20]	−1.2443	−1.2301	−1.2174	−1.4868	−1.3184	−1.30(10)
^{133}Sn	$\frac{7}{2}^-$	[503]7/2	$2f_{7/2}$	−1.410(1)	[Rod20]	−1.5391	−1.5607	−1.5775	−1.6580	−1.5713	−1.58(4)
^{131}In	$\frac{9}{2}^+$	[404]9/2	$1g_{9/2}$	6.312(14)	[Ver21]	6.0340	6.0133	5.9055	6.2650	6.0926	6.06(12)
^{133}Sb	$\frac{7}{2}^+$	[404]7/2	$1g_{7/2}$	3.070(2)	[Lec21]	2.2813	2.1792	2.2088	2.1125	2.1379	2.18(6)
^{207}Pb	$\frac{1}{2}^-$	[501]1/2	$3p_{1/2}$	0.5906(4)	[Adr16]	0.6059	0.6021	0.6129	0.6120	0.5972	0.606(6)
^{209}Pb	$\frac{9}{2}^+$	[604]9/2	$2g_{9/2}$	−1.4735(16)	[Sto05]	−1.5270	−1.5539	−1.6222	−1.6556	−1.5664	−1.59(5)
^{207}Tl	$\frac{1}{2}^+$	[400]1/2	$3s_{1/2}$	1.876(5)	[Sto05]	2.5797	2.6036	2.6051	2.6475	2.6135	2.61(2)
^{209}Bi	$\frac{9}{2}^-$	[505]9/2	$1h_{9/2}$	4.092(2)	[Skr18]	3.2065	3.1027	3.1249	3.0136	3.0522	3.10(7)

*sign not measured; calculated sign was assigned.

**functional SkO′ excluded.

Table 9.1: Experimental values of the magnetic dipole moments μ of the ground states compared with those calculated for functionals UNEDF1, SLy4, SkO′, D1S, and N^{3}LO [Sas22].

				Electric quadrupole moment Q (b)							
Nuclide	I^π	$[Nn_z\Lambda]K$	orbital	EXP	Ref.	UNEDF1	SLy4	SkO′	D1S	N^{3}LO	Average
^{17}O	$\frac{5}{2}^+$	[202]5/2	$1d_{5/2}$	−0.0256(2)*	[Sto16]	−0.0108	−0.0087	−0.0086	−0.0085	−0.0098	−0.0093(9)
^{17}F	$\frac{5}{2}^+$	[202]5/2	$1d_{5/2}$	−0.076(4)*	[Sto16]	−0.0712	−0.0721	−0.0720	−0.0730	−0.0691	−0.0715(13)
^{39}Ca	$\frac{3}{2}^+$	[202]3/2	$1d_{3/2}$	0.036(7)	[Sto16]	0.0075	0.0070	0.0070	0.0073	0.0072	0.0072(2)
^{41}Ca	$\frac{7}{2}^-$	[303]7/2	$1f_{7/2}$	−0.0665(18)	[Sto16]	−0.0323	−0.0270	−0.0270	−0.0263	−0.0288	−0.028(2)
^{39}K	$\frac{3}{2}^+$	[202]3/2	$1d_{3/2}$	0.0585(6)	[Sto16]	0.0546	0.0580	0.0565	0.0576	0.0555	0.0564(13)
^{41}Sc	$\frac{7}{2}^-$	[303]7/2	$1f_{7/2}$	−0.145(3)*	[Sto16]	−0.1199	−0.1255	−0.1218	−0.1266	−0.1211	−0.123(3)
^{47}Ca	$\frac{7}{2}^-$	[303]7/2	$1f_{7/2}$	0.084(6)	[Gar15]	0.0460	0.0395	0.0441	0.0379	0.0415	0.042(3)
^{49}Ca	$\frac{3}{2}^-$	[301]3/2	$2p_{3/2}$	−0.036(3)	[Gar15]	−0.0104	−0.0084	−0.0094	−0.0079	−0.0103	−0.0093(10)
^{49}Sc	$\frac{7}{2}^-$	[303]7/2	$1f_{7/2}$	−0.159(8)	[Bai22]	−0.1545	−0.1455	−0.1496	−0.1408	−0.1393	−0.146(6)
^{55}Ni	$\frac{7}{2}^-$	[303]7/2	$1f_{7/2}$			0.1637	0.1486	0.1661	0.1274	0.1336	0.148(16)
^{57}Ni	$\frac{3}{2}^-$	[301]3/2	$2p_{3/2}$			−0.0685	−0.0511	−0.1622	−0.0434	−0.0518	−0.054(9)**
^{55}Co	$\frac{7}{2}^-$	[303]7/2	$1f_{7/2}$			0.2254	0.2241	0.2371	0.2086	0.2091	0.221(11)
^{57}Cu	$\frac{3}{2}^-$	[301]3/2	$2p_{3/2}$			−0.1207	−0.1143	−0.1919	−0.1077	−0.1096	−0.113(5)**
^{77}Ni	$\frac{9}{2}^+$	[404]9/2	$1g_{9/2}$			0.1600	0.1305	0.1555	0.1197	0.1275	0.139(16)
^{79}Ni	$\frac{5}{2}^+$	[402]5/2	$2d_{5/2}$			−0.0797	−0.0601	−0.0825	−0.0513	−0.0581	−0.066(13)
^{77}Co	$\frac{7}{2}^-$	[303]7/2	$1f_{7/2}$			0.2075	0.1847	0.2121	0.1874	0.1778	0.194(13)
^{79}Cu	$\frac{3}{2}^-$	[301]3/2	$2p_{3/2}$			−0.1033	−0.0962	−0.0853	−0.0940	−0.0910	−0.094(6)
^{99}Sn	$\frac{9}{2}^+$	[404]9/2	$1g_{9/2}$			0.1719	0.1628	0.1773	0.1507	0.1575	0.164(10)
^{101}Sn	$\frac{5}{2}^+$	[402]5/2	$2d_{5/2}$			−0.0927	−0.0842		−0.0788	−0.0920	−0.0870(6)**
^{99}In	$\frac{9}{2}^+$	[404]9/2	$1g_{9/2}$			0.2848	0.2935	0.3040	0.2865	0.2848	0.291(7)
^{101}Sb	$\frac{7}{2}^+$	[404]7/2	$1g_{7/2}$			−0.2936	−0.2975	−0.2858	−0.2921	−0.2903	−0.292(4)
^{131}Sn	$\frac{11}{2}^-$	[505]11/2	$1h_{11/2}$	0.203(4)	[Yor20]	0.1737	0.1616	0.1780	0.1507	0.1596	0.165(10)
^{133}Sn	$\frac{7}{2}^-$	[503]7/2	$2f_{7/2}$	−0.145(10)	[Rod20]	−0.0919	−0.0845	−0.0979	−0.0815	−0.0941	−0.090(6)
^{131}In	$\frac{9}{2}^+$	[404]9/2	$1g_{9/2}$	0.31(1)	[Ver21]	0.2615	0.2664	0.2815	0.2712	0.2589	0.268(8)
^{133}Sb	$\frac{7}{2}^+$	[404]7/2	$1g_{7/2}$	−0.304(7)	[Lec21]	−0.2549	−0.2566	−0.2503	−0.2609	−0.2508	−0.255(4)
^{209}Pb	$\frac{9}{2}^+$	[604]9/2	$2g_{9/2}$	−0.27(17)	[Sto16]	−0.1514	−0.1450	−0.1348	−0.1325	−0.1510	−0.143(8)
^{209}Bi	$\frac{9}{2}^-$	[505]9/2	$1h_{9/2}$	−0.47(5)***	[Sto16; Skr21]	−0.3710	−0.3736	−0.3661	−0.3835	−0.3643	−0.372(7)

*sign not measured; calculated sign was assigned.

**functional SkO′ excluded.

***average of −0.516(15) [Sto16] and −0.418(6) [Skr21] with the error bar reflecting uncertainties of the atomic theory.

Table 9.2: Experimental values of the electric quadrupole moments Q of the ground states compared with those calculated for functionals UNEDF1, SLy4, SkO′, D1S, and N^{3}LO [Sas22].

In Figure (9.1) we show all the data from our calculations of the quadrupole and dipole moments compared with currently available experimental data. It can be easily seen that our approach of using DFT is successful in producing the data without the use of effective charges or g-factors.

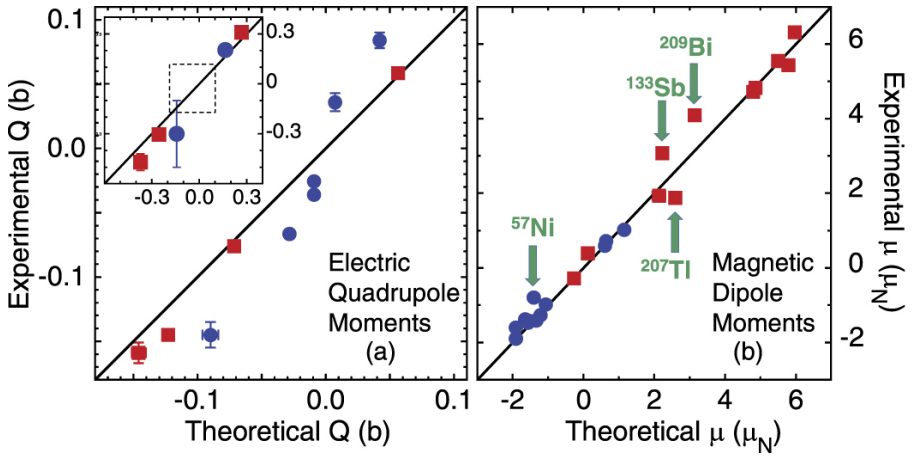

Figure 9.1: Calculated electric quadrupole moments Q, panel (a), compared with 15 experimentally measured values (the inset shows values that are outside the area of the main plot, as visualized by the dashed-line square drawn inside). Panel (b) shows analogous results obtained for the magnetic dipole moments μ compared with 23 experimentally measured values (the arrows mark the outlier cases discussed in the text). Full circles (squares) show results obtained for N-odd (Z-odd) nuclei. Calculated values shown in this figure were derived within the Bayesian Model Averaging (BMA) analysis. Apart from one point, the corresponding theoretical error bars are always smaller than the sizes of symbols [Sas22].

In Figure (9.2) we show the full dependence of the parameter g_0' on the spin magnetic dipole moment $|\mu^{\mathrm{S}}|$ for the UNEDF1 functional. As discussed in Chapter 3.1, using the spin magnetic moments, we are able to compare our results in a simple manner. We have also shown in Figure (9.3) the dependence with the residuals $\mu_{\mathrm{the}} - \mu_{\mathrm{exp}}$ which helps to visualise how the parameter effects the moments.

In Figures (9.2) and (9.3), we have 3 distinct groups of nuclei that we have seperated using solid, dashed and dotted lines.

The first group (dashed lines in Figure (9.2)) contains the eight lightest nuclei around ^{16}O and ^{40}Ca, which are characterized by all spin-orbit partners located on the same side of the Fermi energy. In these nuclei, irrespective of whether an odd proton or an odd neutron, or a hole or particle state, or a high or low spin state are occupied, no tangible polarisation of the spin distribution is obtained and no ensuing dependence of the magnetic dipole moment on the isovector spin-spin interaction is visible. As a result, in this group, all magnetic dipole

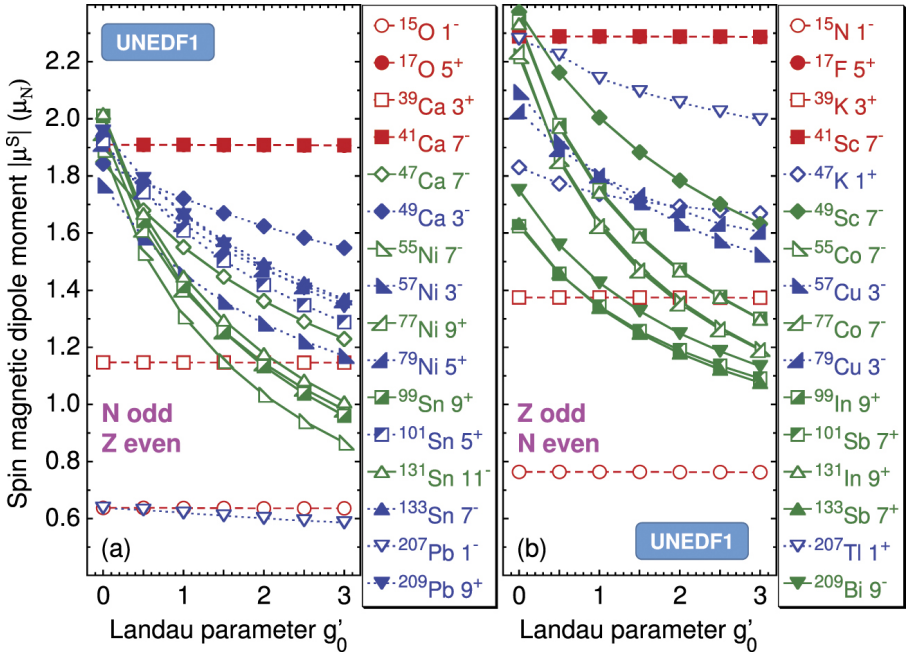

Figure 9.2: Absolute values of the UNEDF1 spin magnetic dipole moments $|\mu^{\mathrm{S}}|$ calculated in function of the Landau parameter g_0' for N-odd-Z-even (a) and Z-odd-N-even (b) nuclei. Dashed, solid, and dotted lines denote nuclei belonging to the first, second, and third group discussed in the text, respectively. Values obtained for ^{17}O and ^{17}F are hidden behind those obtained for ^{41}Ca and ^{41}Sc, respectively. Doubled ground-state spin and parity are given in the legends. Full and empty symbols denote particle and hole states, respectively [Sas22].

moments stay quite rigidly fixed at the Schmidt limits shown in Figure (3.1).

The second group (solid lines in Figures (9.2) and (9.3)) contains nuclei around heavier doubly magic nuclei, which are characterized by the Fermi energies separating pairs of the spin-orbit partners from one another, and by a hole or a particle created in one of the spin-orbit partners. In all such nuclei, irrespective of whether the nucleus contains an odd-proton or an odd-neutron, the dependence of the magnetic dipole moments on the isovector spin-spin interaction is strong. Two exceptions from this rule are the cases of ^{47}Ca and ^{49}Sc, where only the neutron pair of spin-orbit partners is available for polarisation and the response to the isovector spin-spin interaction is somewhat weaker. With increasing values of g_0', the calculated magnetic dipole moments significantly depart from the Schmidt limits.

Finally, the third group (dotted lines in Figures (9.2)) contains nuclei in which particles or holes are created in non-intruder states or their partners. Then, the spin polarisation of the spin-orbit partners becomes weaker and, as a result, the dependence of the magnetic dipole moments on the isovector spin-spin interaction weakens too. For $\frac{1}{2}^{\pm}$ states, such dependence is particularly weak.

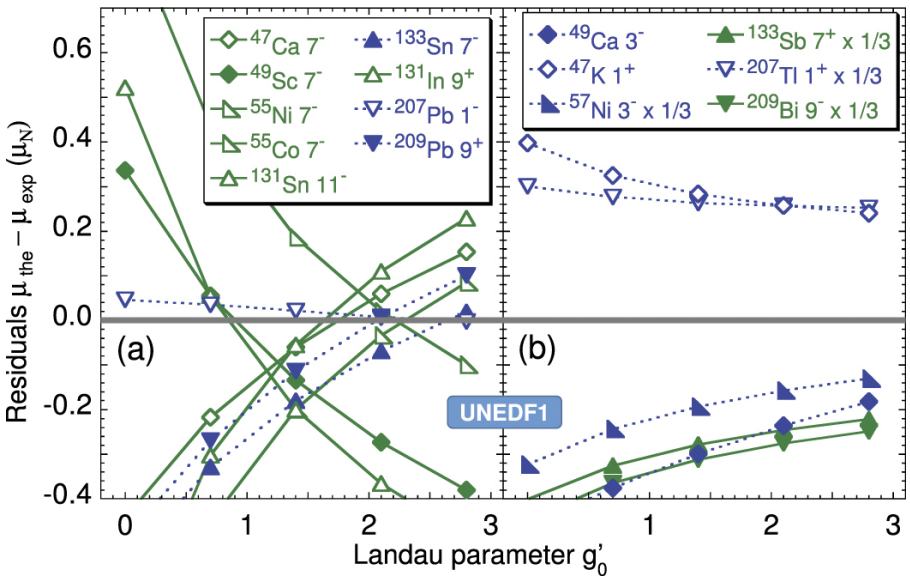

Figure 9.3: The UNEDF1 magnetic dipole moments μ calculated in function of the Landau parameter g_0' relative to the experimental values. Panels (a) and (b) show results that do and do not cross the line of $\mu_{\text{the}} = \mu_{\text{exp}}$, respectively. Solid and dotted lines denote nuclei belonging to the second and third group discussed in the text, respectively. Symbols $\times 1/3$ denote outlier values multiplied by a factor of 1/3 to fit in the scale of the figure [Sas22].

From the other two Skyrme functionals used, SLy4 and SkO′, the same pattern of dependence was recognised for the dipole moment with respect to the Landau parameter. We show this in Figure (9.4(a)) by plotting the RMS deviations of all Skyrme functionals and then determining the optimal values for the Landau parameter from the minima of the curves. These were found to be $g_0' = 1.0$, 1.3, and 1.7 for SkO′, SLy4, and UNEDF1, respectively.

In Figure (9.5) we present a full results for only the UNEDF1, the D1S and the N^3LO functionals using the previously determined optimal values for the Landau parameter g_0', where we have plotted the spin magnetic dipole moment $|\mu^{\text{S}}|$ for all the nuclei aand compared them with the Schmidt values and experimental data.

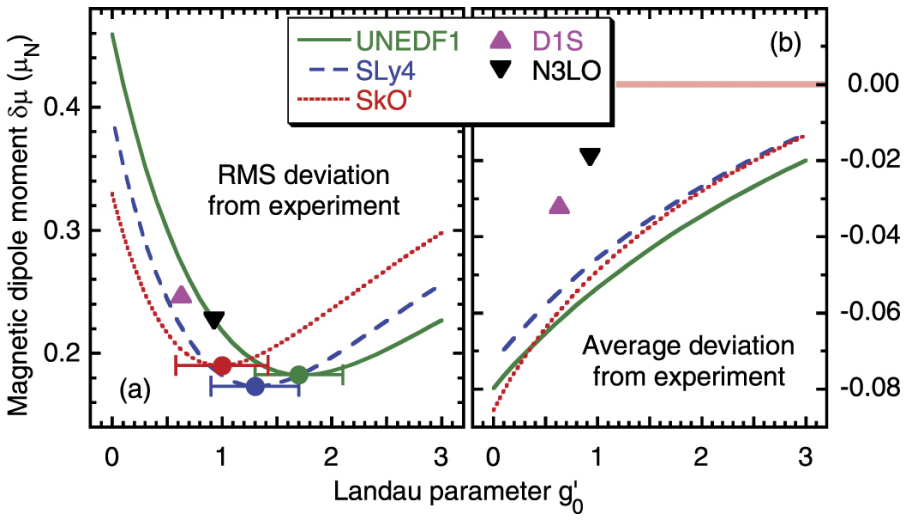

Figure 9.4: RMS (a) and average (b) deviations $\delta\mu$ between the calculated and experimental values of magnetic dipole moments [Sas22].

As seen in Figure (9.6) we show values of the effective spin g-factors g_{eff} that would need to be used for each nuclei in order to reproduce the experimental values of the magnetic dipole moments μ for the UNEDF1 functional. This effective spin g-factor is an addition to the spin gyromagnetic factors in Equation (3.2) where they are mulitplied together to better reproduce experimental data:

$$g_s^n = -3.826\,\mu_N \times g_{\text{eff}}, \quad g_s^p = +5.586\,\mu_N \times g_{\text{eff}}. \tag{9.1}$$

From our work, we can confidently say that our method does not support the need for any effective spin g-factors to reproduce the magnetic dipole moments for atomic nuclei. Further analysis shows that if we were to introduce this g-factor, a value of $g_{\text{eff}} = 0.98(10)$ would be needed, with the outlier cases (dashed circles in Figure (9.6)) not included. For these outliers a value of $g_{\text{eff}} \leq 0.7$ would be needed and raises the question of additional methods in our approach to explain this discrepancy.

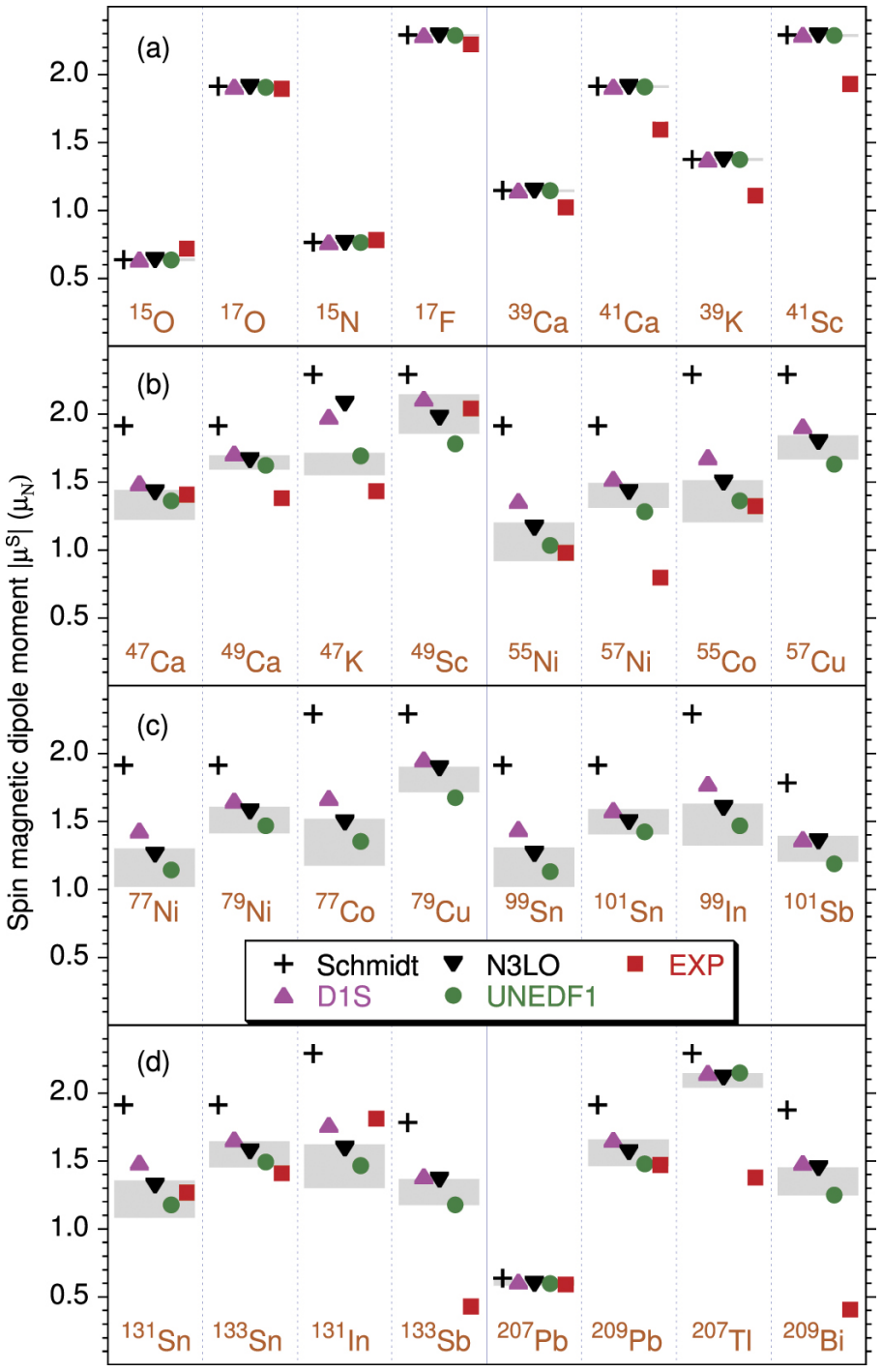

Figure 9.5: Absolute values of the spin magnetic moments $|\mu^S|$ calculated for D1S, N^{3}LO and UNEDF1 functionals and compared with the Schmidt values and experimental data [Sas22].

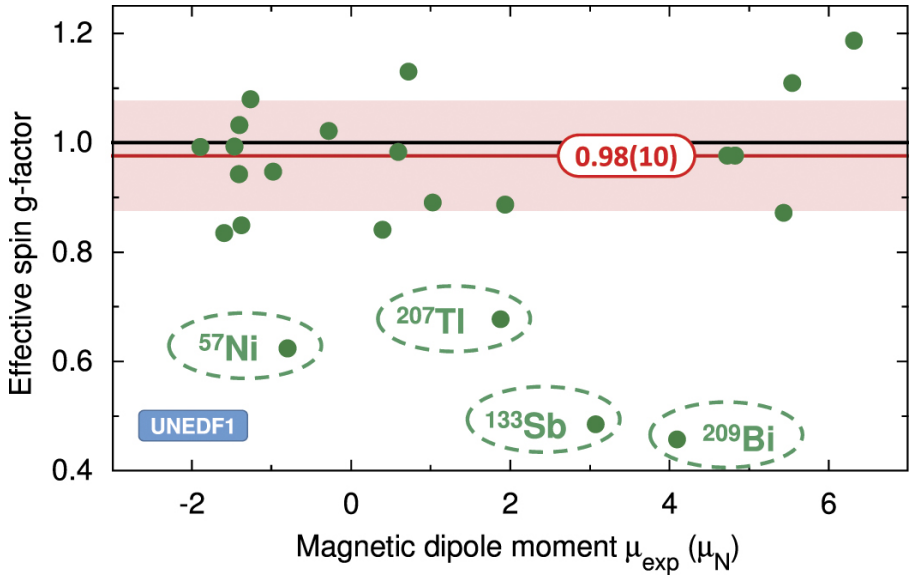

Figure 9.6: Effective spin g-factors g_{eff} that would have been needed for bringing the calculated UNEDF1 magnetic dipole moments μ to the 23 experimentally measured values [Sas22].

9.2 Excited States

Further calculations were done, using an almost identical procedure to the ground states, as theoretical predictions for magnetic dipole moments μ and electric quadrupole moments Q of so called excited states as there is currently no experimental data available. We occupied all the single-particle states of one shell above and depopulated all one-hole states of one shell below the closed shells for the doubly magic nuclei. This was achieved by specifying which states we wish to occupy/depopulate using the Nilsson plots in Chapter 2.2 to confirm the single-particle levels. In Tables (9.3) and (9.4) we show the magnetic dipole moments and in Tables (9.5) and (9.6) we show the electric quadrupole moments for the UNEDF1 functional only using $g_0' = 1.7$. The tables include the Nilsson labels for each with the occupied orbitals and spin and parity of the level. It should be noted that we were unable to get converge solutions for four nuclei; ^{57}Ni($\frac{5}{2}^-$), ^{57}Cu($\frac{5}{2}^-$), ^{79}Ni($\frac{7}{2}^+$) and ^{79}Ni($\frac{11}{2}^-$). It is suspected that configuration mixing may be a factor for the unstable solutions of the nuclei.

				μ (μ_N)					μ (μ_N)
Nuclide	I^π	$[Nn_z\Lambda]K$	orbital	UNEDF1	Nuclide	I^π	$[Nn_z\Lambda]K$	orbital	UNEDF1
^{15}O	$\frac{3}{2}^-$	[101]3/2	$1p_{3/2}$	-1.9073	^{55}Ni	$\frac{1}{2}^+$	[220]1/2	$2s_{1/2}$	-0.6149
^{17}O	$\frac{1}{2}^+$	[200]1/2	$2s_{1/2}$	-1.9107	^{55}Ni	$\frac{3}{2}^+$	[202]3/2	$1d_{3/2}$	0.8265
^{15}N	$\frac{3}{2}^-$	[101]3/2	$1p_{3/2}$	3.7871	^{55}Ni	$\frac{5}{2}^+$	[202]5/2	$1d_{5/2}$	-1.2159
^{17}F	$\frac{1}{2}^+$	[200]1/2	$2s_{1/2}$	2.7909	^{57}Ni	$\frac{1}{2}^-$	[301]1/2	$2p_{1/2}$	0.5617
^{39}Ca	$\frac{1}{2}^+$	[200]1/2	$2s_{1/2}$	-1.9088	^{57}Ni	$\frac{9}{2}^+$	[404]9/2	$1g_{9/2}$	-0.5102
^{39}Ca	$\frac{5}{2}^+$	[202]5/2	$1d_{5/2}$	-1.9086	^{55}Co	$\frac{1}{2}^+$	[200]1/2	$2s_{1/2}$	2.486
^{41}Ca	$\frac{1}{2}^-$	[301]1/2	$2p_{1/2}$	0.6371	^{55}Co	$\frac{3}{2}^+$	[202]3/2	$1d_{3/2}$	0.4702
^{41}Ca	$\frac{3}{2}^-$	[301]3/2	$2p_{3/2}$	-1.9101	^{55}Co	$\frac{5}{2}^+$	[202]5/2	$1d_{5/2}$	4.0466
^{41}Ca	$\frac{5}{2}^-$	[303]5/2	$1f_{5/2}$	1.3674	^{57}Cu	$\frac{1}{2}^-$	[301]1/2	$2p_{1/2}$	-0.2194
^{41}Ca	$\frac{9}{2}^-$	[404]9/2	$1g_{9/2}$	-1.9074	^{57}Cu	$\frac{9}{2}^+$	[404]9/2	$1g_{9/2}$	5.3005
^{39}K	$\frac{1}{2}^+$	[200]1/2	$2s_{1/2}$	2.789	^{77}Ni	$\frac{1}{2}^-$	[301]1/2	$2p_{1/2}$	0.6009
^{39}K	$\frac{5}{2}^+$	[202]5/2	$1g_{5/2}$	4.7884	^{77}Ni	$\frac{3}{2}^-$	[301]3/2	$2p_{3/2}$	-1.5235
^{41}Sc	$\frac{1}{2}^-$	[301]1/2	$2p_{1/2}$	-0.2638	^{77}Ni	$\frac{5}{2}^-$	[303]5/2	$1f_{5/2}$	0.9795
^{41}Sc	$\frac{3}{2}^-$	[301]3/2	$2p_{3/2}$	3.7905	^{77}Ni	$\frac{7}{2}^-$	[303]7/2	$1f_{7/2}$	-1.2481
^{41}Sc	$\frac{5}{2}^-$	[303]5/2	$1f_{5/2}$	0.8614	^{79}Ni	$\frac{1}{2}^+$	[400]1/2	$3s_{1/2}$	-1.784
^{41}Sc	$\frac{9}{2}^+$	[404]9/2	$1g_{9/2}$	6.7875	^{79}Ni	$\frac{3}{2}^+$	[402]3/2	$2d_{3/2}$	1.0159
^{47}Ca	$\frac{1}{2}^+$	[200]1/2	$2s_{1/2}$	-1.7024	^{77}Co	$\frac{1}{2}^+$	[200]1/2	$2s_{1/2}$	2.4814
^{47}Ca	$\frac{3}{2}^+$	[202]3/2	$1d_{3/2}$	0.9562	^{77}Co	$\frac{3}{2}^+$	[202]3/2	$1d_{3/2}$	0.447
^{47}Ca	$\frac{5}{2}^+$	[202]5/2	$1d_{5/2}$	-1.4493	^{77}Co	$\frac{5}{2}^+$	[202]5/2	$1d_{5/2}$	4.0537
^{49}Ca	$\frac{1}{2}^-$	[301]1/2	$2p_{1/2}$	0.6096	^{79}Cu	$\frac{1}{2}^-$	[301]1/2	$2p_{1/2}$	-0.193
^{49}Ca	$\frac{5}{2}^-$	[303]5/2	$1f_{5/2}$	1.0542	^{79}Cu	$\frac{5}{2}^-$	[303]5/2	$1f_{5/2}$	1.4535
^{49}Ca	$\frac{9}{2}^+$	[404]9/2	$1g_{9/2}$	-1.536	^{79}Cu	$\frac{9}{2}^+$	[404]9/2	$1g_{9/2}$	5.4184
^{47}K	$\frac{3}{2}^+$	[202]3/2	$1d_{3/2}$	0.2497					
^{47}K	$\frac{5}{2}^+$	[202]5/2	$1d_{5/2}$	4.4579					
^{49}Sc	$\frac{1}{2}^-$	[301]1/2	$2p_{1/2}$	-0.2341					
^{49}Sc	$\frac{3}{2}^-$	[301]3/2	$2p_{3/2}$	3.5489					
^{49}Sc	$\frac{5}{2}^-$	[303]5/2	$1f_{5/2}$	1.049					
^{49}Sc	$\frac{9}{2}^+$	[404]9/2	$1g_{9/2}$	6.2545					

Table 9.3: Theoretical values of the magnetic dipole moments μ of the excited states for the functional UNEDF1.

				μ (μ_N)					μ (μ_N)
Nuclide	I^π	$[Nn_z\Lambda]K$	orbital	UNEDF1	Nuclide	I^π	$[Nn_z\Lambda]K$	orbital	UNEDF1
^{99}Sn	$\frac{1}{2}^-$	[301]1/2	$2p_{1/2}$	0.5949	^{131}In	$\frac{1}{2}^-$	[301]1/2	$2p_{1/2}$	-0.2209
^{99}Sn	$\frac{3}{2}^-$	[301]3/2	$2p_{3/2}$	-1.5041	^{131}In	$\frac{3}{2}^-$	[301]3/2	$2p_{3/2}$	3.3642
^{99}Sn	$\frac{5}{2}^-$	[303]5/2	$1f_{5/2}$	0.9568	^{131}In	$\frac{5}{2}^-$	[303]5/2	$1f_{5/2}$	1.2903
^{99}Sn	$\frac{7}{2}^-$	[303]7/2	$1f_{7/2}$	-1.2608	^{131}In	$\frac{7}{2}^-$	[303]7/2	$1f_{7/2}$	5.0898
^{101}Sn	$\frac{1}{2}^+$	[400]1/2	$3s_{1/2}$	-1.7238	^{133}Sb	$\frac{1}{2}^+$	[400]1/2	$3s_{1/2}$	2.5782
^{101}Sn	$\frac{3}{2}^+$	[402]3/2	$2d_{3/2}$	0.9373	^{133}Sb	$\frac{3}{2}^+$	[402]3/2	$2d_{3/2}$	0.3677
^{101}Sn	$\frac{7}{2}^+$	[404]7/2	$1g_{7/2}$	0.9578	^{133}Sb	$\frac{5}{2}^+$	[402]5/2	$2d_{5/2}$	4.3117
^{101}Sn	$\frac{11}{2}^-$	[505]11/2	$1h_{11/2}$	-1.2433	^{133}Sb	$\frac{11}{2}^-$	[505]11/2	$1h_{11/2}$	7.1093
^{99}In	$\frac{1}{2}^-$	[301]1/2	$2p_{1/2}$	-0.2221	^{207}Pb	$\frac{3}{2}^-$	[501]3/2	$3p_{3/2}$	-1.6301
^{99}In	$\frac{3}{2}^-$	[301]3/2	$2p_{3/2}$	3.3870	^{207}Pb	$\frac{5}{2}^-$	[503]5/2	$2f_{5/2}$	1.1294
^{99}In	$\frac{5}{2}^-$	[303]5/2	$1f_{5/2}$	1.2913	^{207}Pb	$\frac{7}{2}^-$	[503]7/2	$2f_{7/2}$	-1.5168
^{99}In	$\frac{7}{2}^-$	[303]7/2	$1f_{7/2}$	5.0949	^{207}Pb	$\frac{9}{2}^-$	[505]9/2	$1h_{9/2}$	1.079
^{101}Sb	$\frac{1}{2}^+$	[400]1/2	$3s_{1/2}$	2.6199	^{207}Pb	$\frac{13}{2}^+$	[606]13/2	$1i_{13/2}$	-1.2613
^{101}Sb	$\frac{3}{2}^+$	[402]3/2	$2d_{3/2}$	0.3279	^{209}Pb	$\frac{1}{2}^+$	[600]1/2	$4s_{1/2}$	-1.8021
^{101}Sb	$\frac{5}{2}^+$	[402]5/2	$2d_{5/2}$	4.3508	^{209}Pb	$\frac{3}{2}^+$	[602]3/2	$3d_{3/2}$	1.0216
^{101}Sb	$\frac{11}{2}^-$	[505]11/2	$1h_{11/2}$	7.1124	^{209}Pb	$\frac{3}{2}^+$	[602]5/2	$3d_{5/2}$	-1.6508
^{131}Sn	$\frac{1}{2}^+$	[400]1/2	$3s_{1/2}$	-1.7284	^{209}Pb	$\frac{7}{2}^+$	[604]7/2	$2g_{7/2}$	1.219
^{131}Sn	$\frac{3}{2}^+$	[402]3/2	$2d_{3/2}$	0.9852	^{209}Pb	$\frac{11}{2}^+$	[606]11/2	$1i_{11/2}$	1.094
^{131}Sn	$\frac{5}{2}^+$	[402]5/2	$2d_{5/2}$	-1.5156	^{207}Tl	$\frac{3}{2}^+$	[402]3/2	$2d_{3/2}$	0.297
^{131}Sn	$\frac{7}{2}^+$	[404]7/2	$1g_{7/2}$	1.0424	^{207}Tl	$\frac{5}{2}^+$	[402]5/2	$2d_{5/2}$	4.3495
^{133}Sn	$\frac{1}{2}^-$	[501]1/2	$3p_{1/2}$	0.6104	^{207}Tl	$\frac{7}{2}^+$	[404]7/2	$1g_{7/2}$	2.2108
^{133}Sn	$\frac{3}{2}^-$	[501]3/2	$3p_{3/2}$	0.4463	^{207}Tl	$\frac{11}{2}^-$	[405]11/2	$1h_{11/2}$	7.0651
^{133}Sn	$\frac{5}{2}^-$	[503]5/2	$2f_{5/2}$	1.1491	^{209}Bi	$\frac{1}{2}^-$	[501]1/2	$3p_{1/2}$	-0.1824
^{133}Sn	$\frac{9}{2}^-$	[505]9/2	$1h_{9/2}$	1.0711	^{209}Bi	$\frac{3}{2}^-$	[501]3/2	$3p_{3/2}$	3.4641
^{133}Sn	$\frac{13}{2}^+$	[606]13/2	$1i_{13/2}$	-1.2962	^{209}Bi	$\frac{5}{2}^-$	[503]5/2	$2f_{5/2}$	1.1693
					^{209}Bi	$\frac{7}{2}^-$	[503]7/2	$2f_{7/2}$	5.3239
					^{209}Bi	$\frac{13}{2}^+$	[606]13/2	$1i_{13/2}$	8.1359

Table 9.4: Theoretical values of the magnetic dipole moments μ of the excited states for the functional UNEDF1 (Table 9.3 continued).

				Q (b)					Q (b)
Nuclide	I^π	$[Nn_z\Lambda]K$	orbital	UNEDF1	Nuclide	I^π	$[Nn_z\Lambda]K$	orbital	UNEDF1
^{15}O	$\frac{3}{2}^-$	[101]3/2	$1p_{3/2}$	0.0039	^{55}Ni	$\frac{3}{2}^+$	[202]3/2	$1d_{3/2}$	0.0584
^{15}N	$\frac{3}{2}^-$	[101]3/2	$1p_{3/2}$	0.0305	^{55}Ni	$\frac{3}{2}^+$	[202]3/2	$1d_{3/2}$	0.0984
^{39}Ca	$\frac{5}{2}^+$	[202]5/2	$1d_{5/2}$	0.0183	^{57}Ni	$\frac{9}{2}^+$	[404]9/2	$1g_{9/2}$	-0.6183
^{41}Ca	$\frac{3}{2}^-$	[301]3/2	$2p_{3/2}$	-0.0072	^{55}Co	$\frac{3}{2}^+$	[202]3/2	$1d_{3/2}$	0.0961
^{41}Ca	$\frac{5}{2}^-$	[303]5/2	$1f_{5/2}$	-0.023	^{55}Co	$\frac{5}{2}^+$	[202]5/2	$1d_{5/2}$	0.1498
^{41}Ca	$\frac{9}{2}^-$	[404]9/2	$1g_{9/2}$	-0.0468	^{57}Cu	$\frac{9}{2}^+$	[404]9/2	$1g_{9/2}$	-0.6995
^{39}K	$\frac{5}{2}^+$	[202]5/2	$1g_{5/2}$	0.0758	^{77}Ni	$\frac{3}{2}^-$	[301]3/2	$2p_{3/2}$	0.0283
^{41}Sc	$\frac{3}{2}^-$	[301]3/2	$2p_{3/2}$	-0.0857	^{77}Ni	$\frac{5}{2}^-$	[303]5/2	$1f_{5/2}$	0.0994
^{41}Sc	$\frac{5}{2}^-$	[303]5/2	$1f_{5/2}$	-0.1219	^{77}Ni	$\frac{7}{2}^-$	[303]7/2	$1f_{7/2}$	0.1167
^{41}Sc	$\frac{9}{2}^+$	[404]9/2	$1g_{9/2}$	-0.1775	^{79}Ni	$\frac{3}{2}^+$	[402]3/2	$2d_{3/2}$	-0.0259
^{47}Ca	$\frac{3}{2}^+$	[202]3/2	$1d_{3/2}$	0.0145	^{77}Co	$\frac{3}{2}^+$	[202]3/2	$1d_{3/2}$	0.0884
^{47}Ca	$\frac{5}{2}^+$	[202]5/2	$1d_{5/2}$	0.028	^{77}Co	$\frac{5}{2}^+$	[202]5/2	$1d_{5/2}$	0.138
^{49}Ca	$\frac{5}{2}^-$	[303]5/2	$1f_{5/2}$	-0.0352	^{79}Cu	$\frac{5}{2}^-$	[303]5/2	$1f_{5/2}$	-0.1958
^{49}Ca	$\frac{9}{2}^+$	[404]9/2	$1g_{9/2}$	-0.0669	^{79}Cu	$\frac{9}{2}^+$	[404]9/2	$1g_{9/2}$	-0.4974
^{47}K	$\frac{3}{2}^+$	[202]3/2	$1d_{3/2}$	0.062					
^{47}K	$\frac{5}{2}^+$	[202]5/2	$1d_{5/2}$	0.0949					
^{49}Sc	$\frac{3}{2}^-$	[301]3/2	$2p_{3/2}$	-0.0819					
^{49}Sc	$\frac{5}{2}^-$	[303]5/2	$1f_{5/2}$	-0.1308					
^{49}Sc	$\frac{9}{2}^+$	[404]9/2	$1g_{9/2}$	-0.2151					

Table 9.5: Theoretical values of the electric quadrupole moments Q of the excited states for the functional UNEDF1.

				Q (b)					Q (b)
Nuclide	I^π	$[Nn_z\Lambda]K$	orbital	UNEDF1	Nuclide	I^π	$[Nn_z\Lambda]K$	orbital	UNEDF1
^{99}Sn	$\frac{3}{2}^-$	[301]3/2	$2p_{3/2}$	0.0251	^{207}Pb	$\frac{3}{2}^-$	[501]3/2	$3p_{3/2}$	0.025
^{99}Sn	$\frac{5}{2}^-$	[303]5/2	$1f_{5/2}$	0.0984	^{207}Pb	$\frac{5}{2}^-$	[503]5/2	$2f_{5/2}$	0.073
^{99}Sn	$\frac{7}{2}^-$	[303]7/2	$1f_{7/2}$	0.1045	^{207}Pb	$\frac{7}{2}^-$	[503]7/2	$2f_{7/2}$	0.1065
^{101}Sn	$\frac{3}{2}^+$	[402]3/2	$2d_{3/2}$	-0.0259	^{207}Pb	$\frac{9}{2}^-$	[505]9/2	$1h_{9/2}$	0.1868
^{101}Sn	$\frac{7}{2}^+$	[404]7/2	$1g_{7/2}$	-0.1732	^{207}Pb	$\frac{13}{2}^+$	[606]13/2	$1i_{13/2}$	0.2245
^{101}Sn	$\frac{11}{2}^-$	[505]11/2	$1h_{11/2}$	-0.2479	^{209}Pb	$\frac{3}{2}^+$	[602]3/2	$3d_{3/2}$	-0.0195
^{99}In	$\frac{3}{2}^-$	[301]3/2	$2p_{3/2}$	0.094	^{209}Pb	$\frac{3}{2}^+$	[602]5/2	$3d_{5/2}$	-0.0637
^{99}In	$\frac{5}{2}^-$	[303]5/2	$1f_{5/2}$	0.1837	^{209}Pb	$\frac{7}{2}^+$	[604]7/2	$2g_{7/2}$	-0.1094
^{99}In	$\frac{7}{2}^-$	[303]7/2	$1f_{7/2}$	0.2137	^{209}Pb	$\frac{11}{2}^+$	[606]11/2	$1i_{11/2}$	-0.2401
^{101}Sb	$\frac{3}{2}^+$	[402]3/2	$2d_{3/2}$	-0.131	^{207}Tl	$\frac{3}{2}^+$	[402]3/2	$2d_{3/2}$	0.1336
^{101}Sb	$\frac{5}{2}^+$	[402]5/2	$2d_{5/2}$	-0.2068	^{207}Tl	$\frac{5}{2}^+$	[402]5/2	$2d_{5/2}$	0.205
^{101}Sb	$\frac{11}{2}^-$	[505]11/2	$1h_{11/2}$	-0.393	^{207}Tl	$\frac{7}{2}^+$	[404]7/2	$1g_{7/2}$	0.2826
^{131}Sn	$\frac{3}{2}^+$	[402]3/2	$2d_{3/2}$	2.5345	^{207}Tl	$\frac{11}{2}^-$	[405]11/2	$1h_{11/2}$	0.3742
^{131}Sn	$\frac{5}{2}^+$	[402]5/2	$2d_{5/2}$	0.0593	^{209}Bi	$\frac{3}{2}^-$	[501]3/2	$3p_{3/2}$	-0.1427
^{131}Sn	$\frac{7}{2}^+$	[404]7/2	$1g_{7/2}$	0.1293	^{209}Bi	$\frac{5}{2}^-$	[503]5/2	$2f_{5/2}$	-0.2463
^{133}Sn	$\frac{3}{2}^-$	[501]3/2	$3p_{3/2}$	0.0193	^{209}Bi	$\frac{7}{2}^-$	[503]7/2	$2f_{7/2}$	-0.2922
^{133}Sn	$\frac{5}{2}^-$	[503]5/2	$2f_{5/2}$	-0.0611	^{209}Bi	$\frac{13}{2}^+$	[606]13/2	$1i_{13/2}$	-0.4495
^{133}Sn	$\frac{9}{2}^-$	[505]9/2	$1h_{9/2}$	-0.1711					
^{133}Sn	$\frac{13}{2}^+$	[606]13/2	$1i_{13/2}$	-0.2086					
^{131}In	$\frac{3}{2}^-$	[301]3/2	$2p_{3/2}$	0.0999					
^{131}In	$\frac{5}{2}^-$	[303]5/2	$1f_{5/2}$	0.1742					
^{131}In	$\frac{7}{2}^-$	[303]7/2	$1f_{7/2}$	0.2034					
^{133}Sb	$\frac{3}{2}^+$	[402]3/2	$2d_{3/2}$	-0.1202					
^{133}Sb	$\frac{5}{2}^+$	[402]5/2	$2d_{5/2}$	-0.1804					
^{133}Sb	$\frac{11}{2}^-$	[505]11/2	$1h_{11/2}$	-0.3456					

Table 9.6: Theoretical values of the electric quadrupole moments Q of the excited states for the functional UNEDF1 (Table 9.5 continued).

Chapter 10

Conclusions

In our approach we have shown that nuclear DFT can accurately describe the electric quadrupole and magnetic dipole moments in one-particle and one-hole neighbours of doubly magic nuclei. As we have not constrained our work to specific regions of the nuclear landscape, we can confidently say that we have developed a global desciption baseline for these moments. This was achieved by adjusting one coupling constant in the time-odd mean-field sector of the functional. It should be emphasised that we were able to reproduce such results without the need for effective spin g-factors. These results now provide a perfect base for further work into the time-odd mean-field sector, which may eliminate the outliers we found in our research. Work has already taken place using our approach as a basis to calculate nuclear moments of paired states in nuclei [Bon23].

Appendix A

Wigner-Eckart Theorem

The Wigner-Eckart theorem is a mathematical tool that allows for the separation of the geometric/directional part (projection quantum numbers) and radial/spatial properties of the operators and wavefunctions [BS15].

The theorem states, given a spherical tensor operator $\hat{T}^{(k)}_{\kappa}$ of rank k:

$$\langle JM|\hat{T}^{(k)}_{\kappa}|J'M'\rangle = (-1)^{J-M} \cdot \begin{pmatrix} J & k & J' \\ -M & \kappa & M' \end{pmatrix} \cdot \langle J||\hat{\boldsymbol{T}}^{(k)}||J'\rangle \ . \tag{A.1}$$

From the theorem, a Wigner 3j-symbol and a new matrix element are produced. This new matrix element is called a reduced matrix element. The separation of the parts of the wavefunction is shown by the double bars in the expression above in the reduced matrix element [Hey04].

Appendix B

Second Quantization

We introduce a concept for many-particle systems called second quantization. Emphasis will only be on fermions as we are working with nucleons, however it should be noted that there are equivalent relations for bosons.

We start with generic creation ($\hat{c}^\dagger$) and annihilation ($\hat{c}$) operators. We need expressions that allow us to create and annihilate particles in allowed states. With these operators we wish to change the occupation number (number of particles that can occupy such state), n, which for fermions can be 0 or 1. For normalisation of the these states we are required to have:

$$\langle n|\hat{c}^\dagger\hat{c}|n\rangle = 1 \ . \tag{B.1}$$

However, in our situation we have:

$$\langle n|\hat{c}^\dagger\hat{c}|n\rangle = n \ , \tag{B.2}$$

as in the case of $n = 0$, we will have $\hat{c}$ acting on $|0\rangle$ producing a non-physical state, $|-1\rangle$. We require that $\hat{c}|0\rangle = 0$ and from this we introduce the ansatz, $\hat{c}|n\rangle = \sqrt{n}|n-1\rangle$, hence producing the matrix element [GM96]:

$$\langle n-1|\hat{c}|n\rangle = \sqrt{n} \ , \tag{B.3}$$

and taking the hermitian conjugate of this, we produce,

$$\langle n|\hat{c}^\dagger|n-1\rangle = \sqrt{n} \ . \tag{B.4}$$

From Equations (B.3) and (B.4), it is easily seen that $\hat{c}$ lowers the particle number by 1 and $\hat{c}^\dagger$ raises the particle number by 1.

As we are dealing with fermions, we must abide by the Pauli principle. This means that n can only have the values of 0 or 1, stated earlier. Taking this condition into consideration, it suffices that we cannot act on a state with the same operator twice without it vanishing, therefore it must return 0. We now define such relations to account for this, $\hat{c}^{\dagger 2} = 0$ and $\hat{c}^2 = 0$.

Another condition we must abide by is that particles in different states, the wavefunctions must be anti-symmetric under particle exchange, e.g. $\hat{c}_i^\dagger \hat{c}_j^\dagger = -\hat{c}_j^\dagger \hat{c}_i^\dagger$.

To represent this in a condensed form for all combinations, we can use the anti-commutation relations as follows [GM96]:

$$\{\hat{c}_i, \hat{c}_j\} = 0 \ , \quad \{\hat{c}_i^\dagger, \hat{c}_j^\dagger\} = 0 \ , \quad \{\hat{c}_i, \hat{c}_j^\dagger\} = \delta_{ij} \ . \tag{B.5}$$

We will eventually show that these relations hold true for fermions, however with a notation change defining the creation and/or annihilation of particles, $c \to a$.

Now we define a new operator, $\hat{n}$, the number operator:

$$\hat{n} = \hat{a}^\dagger \hat{a} \ . \tag{B.6}$$

This has the property of returning the number of particles occupying a state and/or the total number of occupied states, dependant on your choice of definition [GM96].

If we compute $\hat{n}^2$, we arrive at the conclusion that the eigenvalues of the number operator can only be 0 or 1, since $\hat{n}^2 = \hat{n}$. Hence, there are only two eigenstates, the vacuum state $|0\rangle$ and the one-particle state $|1\rangle$.

Here we show the action of the operators on such states:

$$\begin{gathered} \hat{n}|0\rangle = 0 \ , \quad \hat{a}^\dagger|0\rangle = |1\rangle \ , \quad \hat{a}|0\rangle = 0 \ , \\ \\ \hat{n}|1\rangle = |1\rangle \ , \quad \hat{a}^\dagger|1\rangle = 0 \ , \quad \hat{a}|1\rangle = |0\rangle \ . \end{gathered} \tag{B.7}$$

We continue by evaluating the matrix elements:

$$\hat{n}|n\rangle = n|n\rangle \ , \quad \hat{a}^\dagger|n\rangle = (1-n)|n+1\rangle \ , \quad \hat{a}|n\rangle = n|n-1\rangle \ . \tag{B.8}$$

And the anti-commutation relations are exactly the same as in (B.5):

$$\{\hat{a}_i, \hat{a}_j\} = 0 \ , \quad \{\hat{a}_i^\dagger, \hat{a}_j^\dagger\} = 0 \ , \quad \{\hat{a}_i, \hat{a}_j^\dagger\} = \delta_{ij} \ . \tag{B.9}$$

Appendix C

Wick's Theorem

Wick's theorem is a technique that is used in which it is possible to simplify a product of annihilation ($\hat{c}$) or creation ($\hat{c}^\dagger$) operators into a sum of product pairs [RS04].

First we begin with defining a contraction:

$$\hat{c}\hat{c}^\dagger = \langle\Psi|\hat{c}\hat{c}^\dagger|\Psi\rangle \ , \tag{C.1}$$

where $|\Psi\rangle$ is the vacuum ($|0\rangle$ for the case of the annihilation and creation operators).

Therefore, we can define the possible contractions:

$$\hat{c}_i\hat{c}_j^\dagger = \langle 0|\hat{c}_i\hat{c}_j^\dagger|0\rangle = \delta_{ij} \ , \tag{C.2}$$

$$\hat{c}_i^\dagger\hat{c}_j = \hat{c}_i^\dagger\hat{c}_j^\dagger = \hat{c}_i\hat{c}_j = 0 \ . \tag{C.3}$$

Hence we can now state Wick's theorem for any product of n fermionic operators O as [Suh07]:

$$\begin{aligned}\langle\Psi|O_1O_2\ldots O_n|\Psi\rangle \ = \ & \sum_{\text{all contraction combinations}} (-1)^{\text{no. of contraction line crossings}} \\ & \times \text{ product with all pairs contracted .}\end{aligned} \tag{C.4}$$

Appendix D

Skyrme Coupling Constants

Here we present all the isoscalar C_0 and isovector C_1 coupling constants from Chapter 6 [Ben02]:

$$C_0^{\rho} = \frac{3}{8}t_0 + \frac{3}{48}t_3\rho_0^{\alpha} \ , \tag{D.1}$$

$$C_1^{\rho} = -\frac{1}{4}t_0(\frac{1}{2} - x_0) - \frac{1}{24}t_3(\frac{1}{2} + x_3)\rho_0^{\alpha} \ , \tag{D.2}$$

$$C_0^{s} = -\frac{1}{4}t_0(\frac{1}{2} - x_0) - \frac{1}{24}t_3(\frac{1}{2} - x_3)\rho_0^{\alpha} \ , \tag{D.3}$$

$$C_1^{s} = -\frac{1}{8}t_0 - \frac{1}{48}t_3\rho_0^{\alpha} \ , \tag{D.4}$$

$$C_0^{\tau} = \frac{3}{16}t_1 + \frac{1}{4}t_2(\frac{5}{4} + x_2) \ , \tag{D.5}$$

$$C_1^{\tau} = -\frac{1}{8}t_1(\frac{1}{2} + x_1) + \frac{1}{8}t_2(\frac{1}{2} + x_2) \ , \tag{D.6}$$

$$C_0^{T} = \eta_J\Big[-\frac{1}{8}t_1(\frac{1}{2} - x_1) + \frac{1}{8}t_2(\frac{1}{2} + x_2)\Big] \ , \tag{D.7}$$

$$C_1^{T} = \eta_J\Big[-\frac{1}{16}t_1 + \frac{1}{16}t_2\Big] \ , \tag{D.8}$$

$$C_0^{\Delta\rho} = -\frac{9}{64}t_1 + \frac{1}{16}t_2(\frac{5}{4} + x_2) \ , \tag{D.9}$$

$$C_1^{\Delta\rho} = \frac{3}{32}t_1(\frac{1}{2} + x_1) + \frac{1}{32}t_2(\frac{1}{2} + x_2) \ , \tag{D.10}$$

$$C_0^{\Delta s} = \frac{3}{32}t_1(\frac{1}{2} - x_1) + \frac{1}{32}t_2(\frac{1}{2} + x_2) \ , \tag{D.11}$$

$$C_1^{\Delta s} = \frac{3}{64}t_1 + \frac{1}{64}t_2 \ , \tag{D.12}$$

$$C_0^{\nabla J} = -\frac{3}{4}W_0 \ , \tag{D.13}$$

$$C_1^{\nabla J} = -\frac{1}{4}W_0 \ , \tag{D.14}$$

$$C_0^{\nabla s} = 0 \ , \tag{D.15}$$

$$C_1^{\nabla s} = 0 \ . \tag{D.16}$$

Bibliography

[Adr16] B. Adrjan et al. "NMR absolute shielding scale and nuclear magnetic dipole moment of ^{207}Pb". In: *Phys. Chem. Chem. Phys.* 18 (24 2016), pp. 16483–16490.

[Ant05] A. Antušek et al. "Nuclear magnetic dipole moments from NMR spectra". In: *Chemical Physics Letters* 411.1 (2005), pp. 111–116. ISSN: 0009-2614.

[Bai22] S. W. Bai et al. "Electromagnetic moments of scandium isotopes and $N = 28$ isotones in the distinctive $0f_{7/2}$ orbit". In: *Physics Letters B* 829 (2022), p. 137064. ISSN: 0370-2693.

[BD21] A. Belyaev and R. Douglas. *The Basics of Nuclear and Particle Physics*. Springer International Publishing, 2021.

[BE16] M. Borrajo and J. L. Egido. "A symmetry-conserving description of odd nuclei with the Gogny force". In: *The European Physical Journal A* 52 (2016). ISSN: 1434-601X.

[BE17] M. Borrajo and J. L. Egido. "Ground-state properties of even and odd Magnesium isotopes in a symmetry-conserving approach". In: *Physics Letters B* 764 (2017), pp. 328–334. ISSN: 0370-2693.

[BE18a] M. Borrajo and J. L. Egido. "Pairing correlations and symmetries in odd-A nuclei." In: *EPJ Web Conf.* 178 (2018), p. 02002.

[BE18b] M. Borrajo and J. L. Egido. "Symmetry conserving configuration mixing description of odd mass nuclei". In: *Phys. Rev. C* 98 (4 Oct. 2018), p. 044317.

[Ben02] M. Bender et al. "Gamow-Teller strength and the spin-isospin coupling constants of the Skyrme energy functional". In: *Phys. Rev. C* 65 (5 May 2002), p. 054322.

[Ben20a] K. Bennaceur et al. "Properties of spherical and deformed nuclei using regularized pseudopotentials in nuclear DFT". In: *Journal of Physics G: Nuclear and Particle Physics* 47 (Aug. 2020), p. 105101.

[Ben20b] K. Bennaceur et al. "Regularized pseudopotential for mean-field calculations". In: *Journal of Physics: Conference Series* 1643 (Dec. 2020), p. 012112.

[Ber09] J. S. Berryman et al. "Doubly-magic nature of ^{56}Ni: Measurement of the ground state nuclear magnetic dipole moment of ^{55}Ni". In: *Phys. Rev. C* 79 (6 2009), p. 064305.

[BGG91] J.F. Berger, M. Girod, and D. Gogny. "Time-dependent quantum collective dynamics applied to nuclear fission". In: *Computer Physics Communications* 63.1 (1991), pp. 365–374.

[Bon12] L. Bonneau et al. "Effect of core polarization on magnetic dipole moments in deformed odd-mass nuclei". In: *Proceedings of the Workshop on Nuclear Theory* 31 (2012), p. 164.

[Bon15] L. Bonneau et al. "Effect of core polarization on magnetic dipole moments in deformed odd-mass nuclei". In: *Phys. Rev. C* 91 (5 May 2015), p. 054307.

[Bon23] J. Bonnard et al. "Nuclear DFT electromagnetic moments in heavy deformed open-shell odd nuclei". In: *Physics Letters B* 843 (2023), p. 138014. ISSN: 0370-2693.

[BS15] D. M. Brink and G. R. Satchler. *Angular Momentum*. Oxford University Press, 2015.

[Cha98] E. Chabanat et al. "A Skyrme parametrization from subnuclear to neutron star densities Part II. Nuclei far from stabilities". In: *Nuclear Physics A* 635.1 (1998), pp. 231–256. ISSN: 0375-9474.

[Co15] G. Co´ et al. "Electric quadrupole and magnetic dipole moments of odd nuclei near the magic ones in a self-consistent approach". In: *Physical Review C* 92.2 (Aug. 2015).

[DD95] J. Dobaczewski and J. Dudek. "Time-odd components in the mean field of rotating superdeformed nuclei". In: *Phys. Rev. C* 52 (4 Oct. 1995), pp. 1827–1839.

[Dob16] J. Dobaczewski et al. "Density functional theory and self-consistent methods". In: *TALENT course lecture notes* (2016).

[dT63] A. de-Shalit and I. Talmi. *Nuclear Shell Theory*. Academic Press, New York, 1963.

[Fir97] R. B. Firestone. *The 8th Edition of The Table of Isotopes*. Wiley-InterScience, 1997.

[Gar15] R. F. Garcia Ruiz et al. "Ground-state electromagnetic moments of calcium isotopes". In: *Phys. Rev. C* 91 (4 2015), p. 041304.

[GM96] W. Greiner and J. A. Maruhn. *Nuclear Models*. Springer-Verlag, 1996.

[Hey04] K. Heyde. *Basic Ideas and Concepts in Nuclear Physics*. Institute of Physics Publishing, 2004.

[Kor12] M. Kortelainen et al. "Nuclear energy density optimization: Large deformations". In: *Phys. Rev. C* 85 (2 Feb. 2012), p. 024304.

[Kra88] K. S. Krane. *Introductory Nuclear Physics*. John Wiley and Sons, 1988.

[KS65] W. Kohn and L. J. Sham. "Self-Consistent Equations Including Exchange and Correlation Effects". In: *Phys. Rev.* 140 (4A Nov. 1965), A1133–A1138.

[Lec21] S. Lechner et al. "Probing the single-particle behavior above ^{132}Sn via electromagnetic moments of ^{133,134}Sb and $N = 82$ isotones". In: *Phys. Rev. C* 104 (1 2021), p. 014302.

[LM18] J. Li and J. Meng. "Nuclear magnetic moments in covariant density functional theory". In: *Frontiers of Physics* 13 (2018). ISSN: 2095-0470.

[McG05] McGraw-Hill. *McGraw-Hill Concise Encyclopedia of Physics*. McGraw-Hill, 2005.

[Ney03] G. Neyens. "Nuclear magnetic and quadrupole moments for nuclear structure research on exotic nuclei". In: *Reports on Progress in Physics* 66.4 (Mar. 2003), pp. 633–689.

[Nil55] S. G. Nilsson. "Binding States of Individual Nucleons in Strongly Deformed Nuclei". In: *Kong. Dan. Vid. Sel. Mat. Fys. Med.* 29N16 (1955), pp. 1–69.

[NIS19] NIST. "CODATA Internationally recommended 2018 values of the Fundamental Physical Constants". In: *The NIST Reference on Constants, Units and Uncertainty* (2019).

[Pér21] S. Péru et al. "Description of magnetic moments within the Gogny Hartree-Fock-Bogolyubov framework: Application to Hg isotopes". In: *Phys. Rev. C* 104 (2 Aug. 2021), p. 024328.

[Rei99] P.G. Reinhard. "Skyrme forces and giant resonances in exotic nuclei". In: *Nucl. Phys. A* 649 (1999), p. 305c.

[Rod20] L. V. Rodríguez et al. "Doubly-magic character of ^{132}Sn studied via electromagnetic moments of ^{133}Sn". In: *Phys. Rev. C* 102 (5 2020), p. 051301.

[RS04] P. Ring and P. Schuck. *The Nuclear Many-Body Problem*. Springer-Verlag, 2004.

[Rut11] E. Rutherford. "The scattering of α and β particles by matter and the structure of the atom". In: *The London, Edinburgh, and Dublin Philosophical Magazine and Journal of Science* 21.125 (1911), pp. 669–688.

[Sas22] P. L. Sassarini et al. "Nuclear DFT Analysis of electromagnetic moments in odd near doubly magic nuclei". In: *Journal of Physics G: Nuclear and Particle Physics* 49.11 (2022), 11LT01.

[Sch37] T. Schmidt. "Über die magnetischen Momente der Atomkerne". In: *Zeitschrift für Physik* 106 (1937), pp. 358–361.

[She21] J. A. Sheikh et al. "Symmetry restoration in mean-field approaches". In: *Journal of Physics G: Nuclear and Particle Physics* 48.12 (Nov. 2021), p. 123001.

[Skr18] L. V. Skripnikov et al. "New Nuclear Magnetic Moment of ^{209}Bi: Resolving the Bismuth Hyperfine Puzzle". In: *Phys. Rev. Lett.* 120 (9 2018), p. 093001.

[Skr21] L. V. Skripnikov et al. "Relativistic Fock space coupled-cluster study of bismuth electronic structure to extract the Bi nuclear quadrupole moment". In: *Phys. Rev. C* 104 (3 2021), p. 034316.

[Sky56] T. H. R. Skyrme. "CVII. The nuclear surface". In: *The Philosophical Magazine: A Journal of Theoretical Experimental and Applied Physics* 1.11 (1956), pp. 1043–1054.

[Sto05] N. J. Stone. "Table of nuclear magnetic dipole and electric quadrupole moments". In: *Atomic Data and Nuclear Data Tables* 90.1 (2005), pp. 75–176. ISSN: 0092-640X.

[Sto16] N. J. Stone. "Table of nuclear electric quadrupole moments". In: *Atomic Data and Nuclear Data Tables* 111-112 (2016), pp. 1–28. ISSN: 0092-640X.

[Suh07] J. Suhonen. *From Nucleons to Nucleus*. Springer, 2007.

[VB72] D. Vautherin and D. M. Brink. "Hartree-Fock Calculations with Skyrme's Interaction. I. Spherical Nuclei". In: *Phys. Rev. C* 5 (3 Mar. 1972), pp. 626–647.

[Ver21] A. R. Vernon et al. "Nuclear moments put a new spin on the structure of ^{131}In". In: *Nature* (2021). submitted.

[VHZ01] K. Vogt, T. Hartmann, and A. Zilges. "Simple parametrization of single- and two-nucleon separation energies in terms of the neutron to proton ratio N/Z". In: *Physics Letters B - PHYS LETT B* 517 (Oct. 2001), pp. 255–260.

[Wei35] C. F. v. Weizsäcker. "Zur Theorie der Kernmassen". In: *Zeitschrift für Physik* 96 (1935), pp. 431–458. ISSN: 0044-3328.

[Wic50] G. C. Wick. "The Evaluation of the Collision Matrix". In: *Phys. Rev.* 80 (2 Oct. 1950), pp. 268–272.

[WLM12] J. Wei, J. Li, and J. Meng. "Relativistic Descriptions of Nuclear Magnetic Moments". In: *Progress of Theoretical Physics Supplement* 196 (Oct. 2012), pp. 400–406. ISSN: 0375-9687.

[WS54] R. D. Woods and D. S. Saxon. "Diffuse Surface Optical Model for Nucleon-Nuclei Scattering". In: *Phys. Rev.* 95 (2 July 1954), pp. 577–578.

[Yor20] D. T. Yordanov et al. "Structural trends in atomic nuclei from laser spectroscopy of tin". In: *Communications Physics* 3.1 (2020), pp. 365–374.